iScience

CellPress
OPEN ACCESS

Article

C-Type Lectins Link Immunological and Reproductive Processes in *Aedes aegypti*

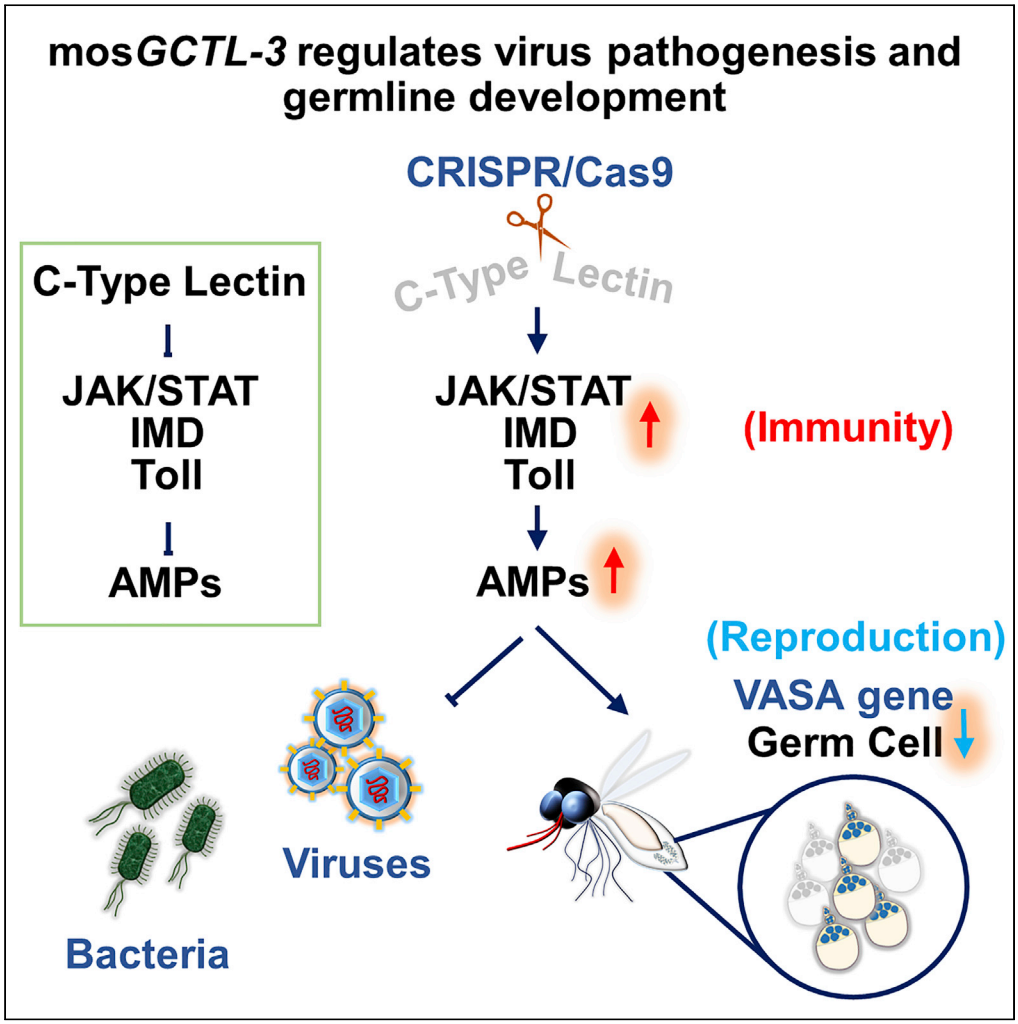

Hsing-Han Li, Yu Cai, Jian-Chiuan Li, ..., Guann-Yi Yu, Horng-Dar Wang, Chun-Hong Chen

chunhong@gmail.com

HIGHLIGHTS

mos*GCTL-3* mutants showed a reduced DENV-2 infection rate

mos*GCTL-3* mutants had upregulated JAK/STAT, IMD, Toll, and AMPs pathway components

mos*GCTL-3* knock-out led to reduced gut microbiota population sizes, and diversity

mos*GCTL-3* regulates germ line development and influences fertility

Li et al., iScience *23*, 101486
September 25, 2020 © 2020
https://doi.org/10.1016/j.isci.2020.101486

iScience

CellPress
OPEN ACCESS

Article

C-Type Lectins Link Immunological and Reproductive Processes in *Aedes aegypti*

Hsing-Han Li,[1,2] Yu Cai,[3,4] Jian-Chiuan Li,[2] Matthew P. Su,[5] Wei-Liang Liu,[6] Lie Cheng,[2] Shu-Jen Chou,[7] Guann-Yi Yu,[2] Horng-Dar Wang,[1] and Chun-Hong Chen[2,6,8,*]

SUMMARY

Physiological trade-offs between mosquito immune response and reproductive capability can arise due to insufficient resource availability. C-type lectin family members may be involved in these processes. We established a *GCTL-3*$^{-/-}$ mutant *Aedes aegypti* using CRISPR/Cas9 to investigate the role of *GCTL-3* in balancing the costs associated with immune responses to arboviral infection and reproduction. *GCTL-3*$^{-/-}$ mutants showed significantly reduced DENV-2 infection rate and gut commensal microbiota populations, as well as upregulated JAK/STAT, IMD, Toll, and AMPs immunological pathways. Mutants also had significantly shorter lifespans than controls and laid fewer eggs due to defective germ line development. dsRNA knock-down of *Attacin* and *Gambicin*, two targets of the AMPs pathway, partially rescued this reduction in reproductive capabilities. Upregulation of immune response following *GCTL-3* knock-out therefore comes at a cost to reproductive fitness. Knock-out of other lectins may further improve our knowledge of the molecular and genetic mechanisms underlying reproduction-immunity trade-offs in mosquitoes.

INTRODUCTION

Physiological trade-offs between immunological response to infection and reproductive ability are likely the result of limited availability of energetic resources (Schwenke et al., 2016). Increased investment in the immune system should therefore result in decreased reproductive capabilities, and vice versa, although there are many other factors that influence the balance of resource allocation (including age and pathogen virulence). Understanding these trade-offs is essential for improving our knowledge of disease-transmitting mosquito species, which are constantly exposed to pathogens during blood feeding and whose egg-laying capabilities are highly relevant in terms of vector control (Delhaye et al., 2016; Flatt and Kawecki, 2007; Miyashita et al., 2019; Simmons, 2011).

Recent publications have highlighted the importance of the mosquito as a site of viral replication and have described methodologies that can inhibit or enhance virus replication within the mosquito itself (Buchman et al., 2019; Wang et al., 2017; Yen et al., 2018). These strategies affect a diverse range of targets but have often resulted in changes to mosquito reproductive potential via unknown mechanisms. Indeed, despite their importance, the wider mechanisms that underlie reproductive/immunological trade-offs remain largely unknown in mosquitoes (Hurd, 2002; Schwenke et al., 2016).

One pathway reported to heavily influence the immune response to infection involves C-type lectins (CTLs), a family of proteins that exhibit carbohydrate-binding activity and have been shown to play vital roles in immune activation and viral pathogenesis (Dambuza and Brown, 2015; Liu et al., 2014; Watanabe et al., 2006). At least 52 C-type lectin domain-containing proteins (CTLDcps) have been annotated in mosquitoes; these have been further categorized as CTLD-S, CTLD-E, CTLD-SP, and CTLD-X. CTLDcps expression levels can vary significantly across developmental stages (Adelman and Myles, 2018). CTLDcps have been identified as important for West Nile virus (WNV) replication and dengue virus (DENV) infection (Adelman and Myles, 2018). The functions of many CTLs remain unclear, however, particularly with regards to Zika virus (ZIKV) infection (Fontes-Garfias et al., 2017; Sirohi and Kuhn, 2017).

[1]Institution of Biotechnology, National Tsing Hua University, Hsinchu, 300044, Taiwan

[2]National Institute of Infectious Diseases and Vaccinology, National Health Research Institutes, Miaoli 350401, Taiwan

[3]Temasek Life Sciences Laboratory, National University of Singapore, 117604, Singapore

[4]Department of Biological Sciences, National University of Singapore, 117558, Singapore

[5]Department of Biological Science, Nagoya University, Nagoya 464-8602, Japan

[6]National Mosquito-Borne Diseases Control Research Center, National Health Research Institutes, Miaoli 350401, Taiwan

[7]Institute of Plant and Microbial Biology, Academia Sinica, Taipei 115201, Taiwan

[8]Lead Contact

*Correspondence: chunhong@gmail.com

https://doi.org/10.1016/j.isci.2020.101486

Many CTLs are employed as receptors or attachment factors to facilitate flavivirus invasion during infection. In previous studies, mosquito *GCTL-1* (mos*GCTL-1*) was shown to be recruited by mosquito protein tyrosine phosphatase-1 (mos*PTP-1*) to allow viral attachment of WNV to cells and facilitate viral entry (Cheng et al., 2010). Mosquito *GCTL-7* (mos*GCTL-7*) has also been reported to bind to the N154 site of N-glycan on the Japanese encephalitis virus envelope protein to promote viral entry into mosquitoes (Liu et al., 2017). Furthermore, two CTLD-S proteins, AAEL0011453 and AAEL012353, are thought to play a key role in gut microbiota homoeostasis and viral entry (Pang et al., 2016). Mosquito *GCTL-3* (mos*GCTL-3*, AAEL000535/AAEL029058), which belongs to the CTLD-S group, can bind to the envelope protein of DENV and assist in the viral infection of host cells. Treating *Aedes* mosquitoes with mos*GCTL-3* antisera was found to be sufficient to block DENV infection (Liu et al., 2014).

Mosquito CTLs also play an important role in maintaining gut microbiome homeostasis, with the microbiome heavily influencing viral replication. In particular, the mosquito gut commensal bacterium, *Serratia marcescens*, secretes the protein *Sm*Enhancin to facilitate arbovirus infection (Wu et al., 2019). *S. marcescens* has also been shown to cause disease in hosts and affect the growth, survival, and development of mosquito larvae (Patil et al., 2011). An abundance of other bacterial genera have additionally been detected in mosquito whole bodies, including *Shigella*, *Asaia*, and *Listeria* (Bertani, 2004; Wasilauskas et al., 1974).

mos*GCTL*s act as immune antagonists that can be utilized by the gut microbiome to escape the bactericidal ability of antimicrobial peptides (AMPs) to protect microbial flora (Pang et al., 2016; Zhang et al., 2017). AMPs expression levels, mediated via the JAK/STAT and Toll pathways, are significantly upregulated in DENV-infected mosquitoes, although DENV-infected cells also decrease the production of AMPs that are mediated via the IMD pathway (Anglero-Rodriguez et al., 2017; Kingsolver et al., 2013; Liu et al., 2012; Xiao et al., 2014; Zhang et al., 2017). The interactions between the different signaling pathways are highly complex and interrelated; further investigation of the influence of CTL family members on the mosquito immune system and gut microbiome composition, as well as the resulting effects on infection rate and transmission, could improve our understanding of these interactions.

We therefore used CRISPR/Cas9 to generate a mos*GCTL-3* knock-out mutant line in *Aedes aegypti*, a major vector of both dengue and ZIKVs (Anglero-Rodriguez et al., 2017; Guzman and Isturiz, 2010; Johansson et al., 2016), with the aim of investigating the trade-offs between immune response and reproduction. mos*GCTL-3* mutants showed a reduction both in DENV-2 and ZIKV prevalence of infection after a blood meal. Mutants also showed elevated JAK/STAT signaling and increased production of specific AMPs, as well as a reduction in gut microbiota, which potentially explains the reduction in DENV-2 prevalence of infection. However, mos*GCTL-3* mutants exhibited compromised germ line development and reduced fertility and were short-lived. Mutant reproductive capabilities were partially restored following dsRNA mediated knock-down of *Attacin* and *Gambicin*, downstream effectors of the AMPs pathway. Production of other CTL knock-out mosquito lines could provide more detail on the functions and mechanisms of this protein family and the role they play in balancing competition for resources between immune response and reproduction.

RESULTS

Generation of *Aedes aegypti GCTL-3* Mutants by CRISPR/Cas9

Mutant generation in many model organisms commonly relies on combining single guide RNA (sgRNA)-mediated deletion with homologous recombination using a donor plasmid containing a selective marker (Supplemental Information, Table S1). Using a similar strategy, we here generated two *GCTL-3* mutants by inserting a cascade containing an *eGFP* gene under the control of a mosquito polyubiquitin promoter into the *GCTL-3* exon region (Figures 1A and 1B, Supplemental Information, Table S2).

To verify the deletion of *GCTL-3* in these mutants, as well as to check for potential off-target effects, we utilized a digital droplet PCR platform to determine the *eGFP* copy number (Figure 1C, Supplemental Information, Table S3). Both heterozygous mutant (*GCTL-3*$^{+/-}$) mosquitoes had a single copy of *GCTL-3* and *eGFP* (Figures 1D and 1E), whereas control mosquitoes had two copies of *GCTL-3* (Figure 1D). We further used genomic PCR and sequencing to confirm that the five potential sgRNA target sites that contained similar sequences to *GCTL-3* were all intact in these two mutants (Supplemental Information, Figure S1A). We also confirmed the recombination site in *GCTL-3* knock-out mutant mosquitoes via PCR and

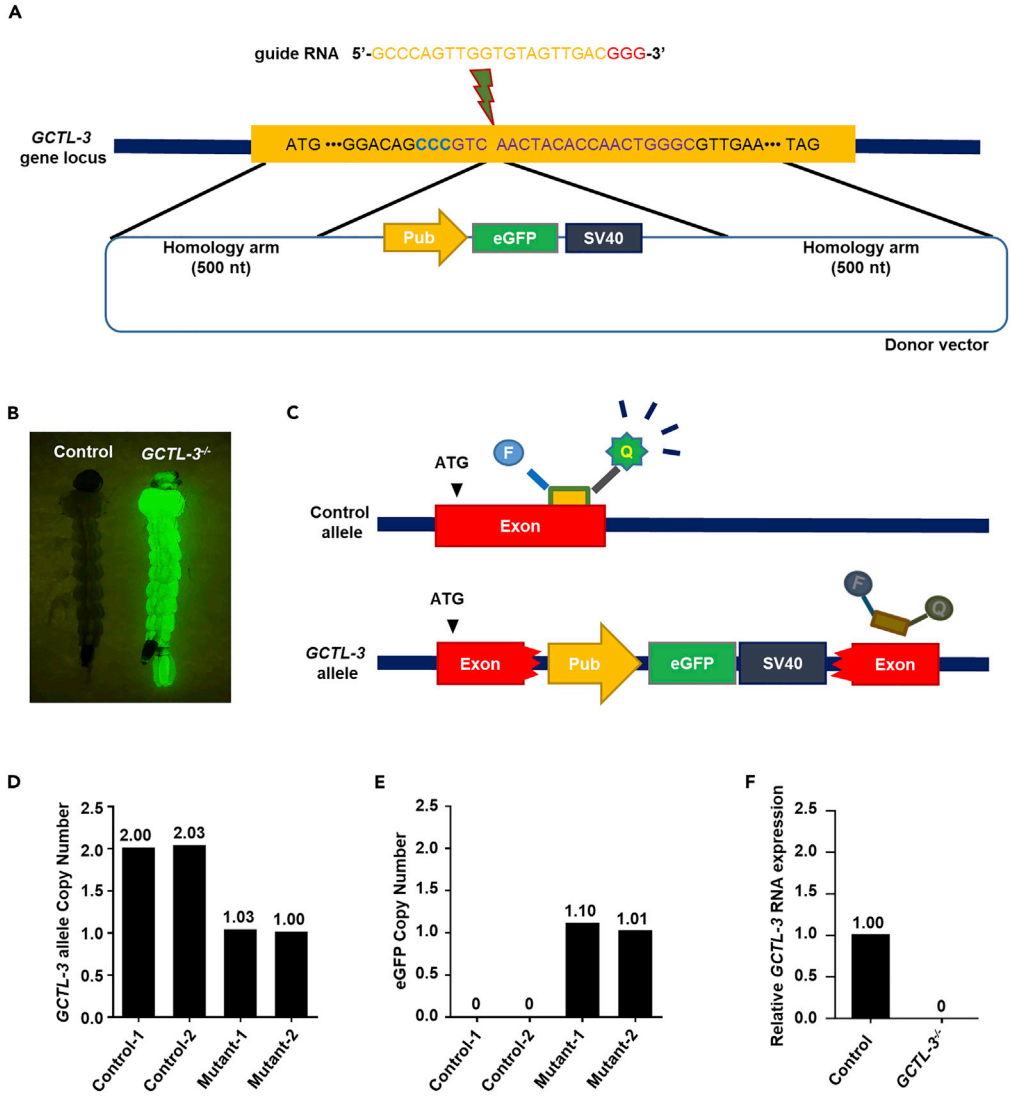

Figure 1. Generation of *Aedes aegypti GCTL-3* Knock-out by CRISPR/Cas9

(A) Schematic of the *A. aegypti GCTL-3* gene locus showing the sgRNA target site (red arrow). Homology arms correspond to sequences immediately adjacent to the predicted cut sites.

(B) Generation of *A. aegypti GCTL-3* gene knock-out mutant mosquitoes: control larvae without fluorescence (left panel); expression of *eGFP* fluorescence in the whole bodies of mutant larvae driven by a poly-ubiquitin (PUb) promoter (right panel).

(C) Schematic of allele-specific detection using TaqMan probes. The designed probe and primer sets for *eGFP* and *GCTL-3* are included in Supplemental Information, Table S3.

(D and E) Copy number variants of (D) mos*GCTL-3* and (E) *eGFP* in control and heterozygote mutant mosquitoes (N=3); data are represented as mean ± SD.

(F) mRNA expression levels of *GCTL-3* in control and mutant mosquitoes (N = 5 each) detected by qPCR across three biological replicates; data are represented as mean ± SD.

See also Tables S1–S3.

sequencing (Supplemental Information, Figures S1B–S1F, Table S4). To investigate the function of *GCTL-3*, we selected one line (mutant-1) and performed outcrossing for five generations to establish the *GCTL-3*$^{-/-}$ homozygous mutant line, and used it throughout this study (Supplemental Information, Figure S2). Homozygous mutant exhibited *eGFP* fluorescence throughout the whole body and did not express detectable *GCTL-3* transcripts (Figure 1F). We then tested heterozygous mosquitoes for fitness and reproductive phenotyping. We found no significant differences between wild-type controls and heterozygous mosquitoes,

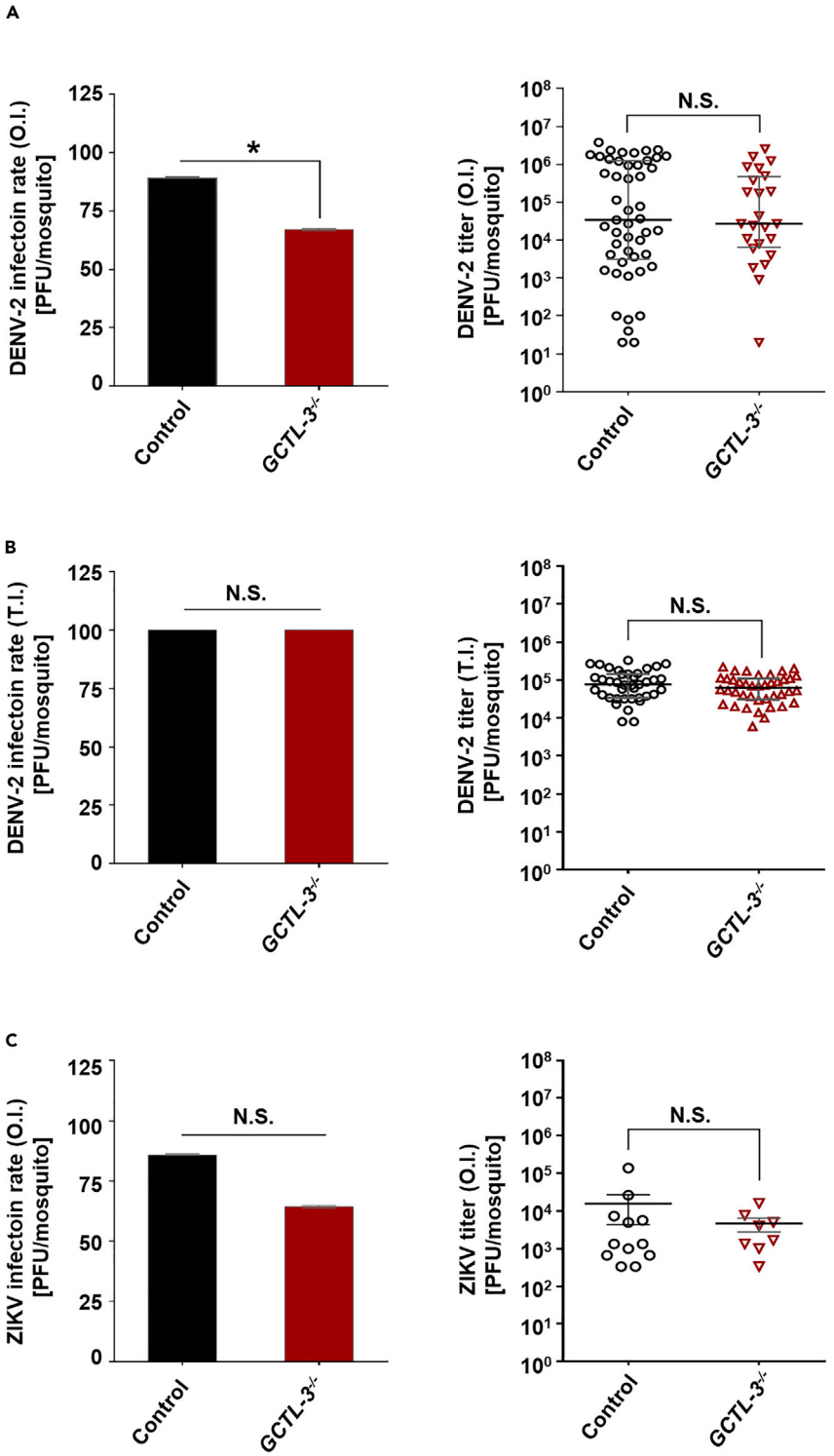

Figure 2. DENV-2, but Not ZIKV, Infection Rate Was Reduced in *GCTL-3*$^{-/-}$ Mosquitoes 7 Days Post-blood Meal

(A–C) Infection rate of (A) DENV-2 and (C) ZIKV in control and *GCTL-3*$^{-/-}$ mosquitoes 7 days post-blood meal and virus titer of (B) DENV-2 in control and *GCTL-3*$^{-/-}$ mosquitoes 7 days post-thoracic injection tested via plaque forming assays in BHK-21 or Vero cells. Sample sizes (DENV-2 for oral infection): Control = 55; *GCTL-3*$^{-/-}$ = 36. Sample sizes (DENV-2 for thoracic injection): Control = 39; *GCTL-3*$^{-/-}$ = 40. Sample sizes (ZIKV for oral infection): Control = 14; *GCTL-3*$^{-/-}$ = 14. Data are represented as mean ± SD for infection rate and represented as median with interquartile range for virus

Figure 2. *Continued*
titer. Asterisks represent significant differences between the genotypes (Mann-Whitney test; *p < 0.05. For infection rate, p = 0.0142 for (A); p > 0.9999 for (B); p = 2087 for (C). For virus titer, p = 0.8179 for (A); p = 0.2062 for (B); p = 0.7185 for (C); raw data related to Figure 2 were indicated in Supplemental Information, Data S1). N.S., no significant difference.

indicating that the possibility of a dominant phenotype due to the pub-EGFP marker was negligible (Supplemental Information, Figure S3 and Data S6).

GCTL-3$^{-/-}$ Mosquitoes Exhibited a Reduced Infection Rate for DENV, but Not ZIKV

To investigate whether GCTL-3 plays a role in arbovirus infection, we first challenged *GCTL-3*$^{-/-}$ mutants with DENV-2 via an artificial membrane blood feeding system and examined virus titers 7 days after this blood meal using plaque formation assay. We found a reduced infection rate for *GCTL-3*$^{-/-}$ mutants compared with controls, with 89% of the control mosquitoes being infected when compared with 67% of mutants (Mann-Whitney test; p = 0.0142). However, we found no significant difference between the groups in terms of viral titer whether it is challenged via oral infection (with median titers of 2.7 × 10^4 plaque-forming unit [PFU]/mL for mutants and 3.4 × 10^4 PFU/mL for controls, Mann-Whitney test; p = 0.8179, Figure 2A) or via thoracic infection (with median titers of 6.3 × 10^4 PFU/mL for mutants and 7.6 × 10^4 PFU/mL for controls, Mann-Whitney test; p = 0.2062, Figure 2B), as detected via plaque assay.

To verify if *GCTL-3* knock-out affected viral titers of other members of the family Flaviviridae, we challenged *GCTL-3*$^{-/-}$ mutants with 1 × 10^6 PFU/mL ZIKV via oral infection. No significant differences were found between mutants and controls in terms of infection rate (64.3% and 85.7%, respectively; Mann-Whitney test; p = 0.2087) or viral titer (with median titers of 2.8 × 10^3 PFU/mL for mutants and 1.3 × 10^3 PFU/mL for controls, Mann-Whitney test; p = 0.7185, Figure 2C).

Reduced Commensal Microbiota Populations in *GCTL-3*$^{-/-}$ Midgut

GCTLs play a substantial role in facilitating colonization of commensal bacteria in the mosquito midgut (Pang et al., 2016). To address whether the knock-out of *GCTL-3* affected the mosquito gut commensal microbiome, we used 16S amplicon sequencing to investigate *GCTL-3*$^{-/-}$ gut microbiota populations. We found that *GCTL-3*$^{-/-}$ mosquitoes had lower overall microbiota populations than controls, with reductions in eight operational taxonomic unit clusters (Figure 3A), as well as increases in two clusters (20% *Dolosigranulum* and 18% *Corynebacterium* compared with controls; data not shown). Fifteen genera were found to have lower levels in *GCTL-3*$^{-/-}$ mutants, including *S. marcescens* and *Salmonella*, common components of the midgut microbiome (Figure 3B). RT-qPCR data provided further evidence that *S. marcescens* abundance was reduced in *GCTL-3*$^{-/-}$ when compared with controls (2.5 × 10^2 colony-forming unit [CFU]/mL and 1.3 × 10^3 CFU/mL respectively) (Figure 3C). In line with these, *GCTL-3*$^{-/-}$ midgut were found to have reduced bacterial DNA levels (Figure 3D) and fewer bacterial colonies than control mosquitoes (Figure 3E), as determined via colony forming assay (1.3 × 10^3 CFU/mL for control and 2.5 × 10^2 CFU/mL for *GCTL-3*$^{-/-}$) (Figure 3F).

Given the previously reported role of *S. marcescens* in facilitating DENV infection, and the adverse effects of this bacterium on other model organisms (Grimont and Grimont, 1978; Kurz et al., 2003; Patil et al., 2011; Wu et al., 2019), we tested the effect on the lifespan of control and mutant mosquitoes when challenged with *S. marcescens* via oral infection. It was observed that 12 days after infection, the survival rates for controls drop significantly from 98% to 85%, whereas the survival rate of *GCTL-3*$^{-/-}$ mutant increased slightly from 91% (untreated) to 94% (treated), consistent with the deleterious effects of *S. marcescens* on mosquitoes. Furthermore, we found a significant interaction between genotype and treatment, indicating that exposing mutants to *S. marcescens* resulted in a significantly different effect on mortality than when exposing controls (p < 0.01) (Figure 3G, Supplemental Information, Table S5).

Activation of JAK/STAT, IMD, Toll, and AMPs Signaling Pathways in *GCTL-3*$^{-/-}$ Mutant Mosquitoes

As upregulation of CTLDcps plays a role in facilitating viral entry and replication via activation of the Toll, IMD, or JAK/STAT pathways and induced AMPs (Jupatanakul et al., 2017; Kingsolver et al., 2013; Xi et al., 2008), we investigated the effect of *GCTL-3* knock-out on these signaling pathways. We found that many

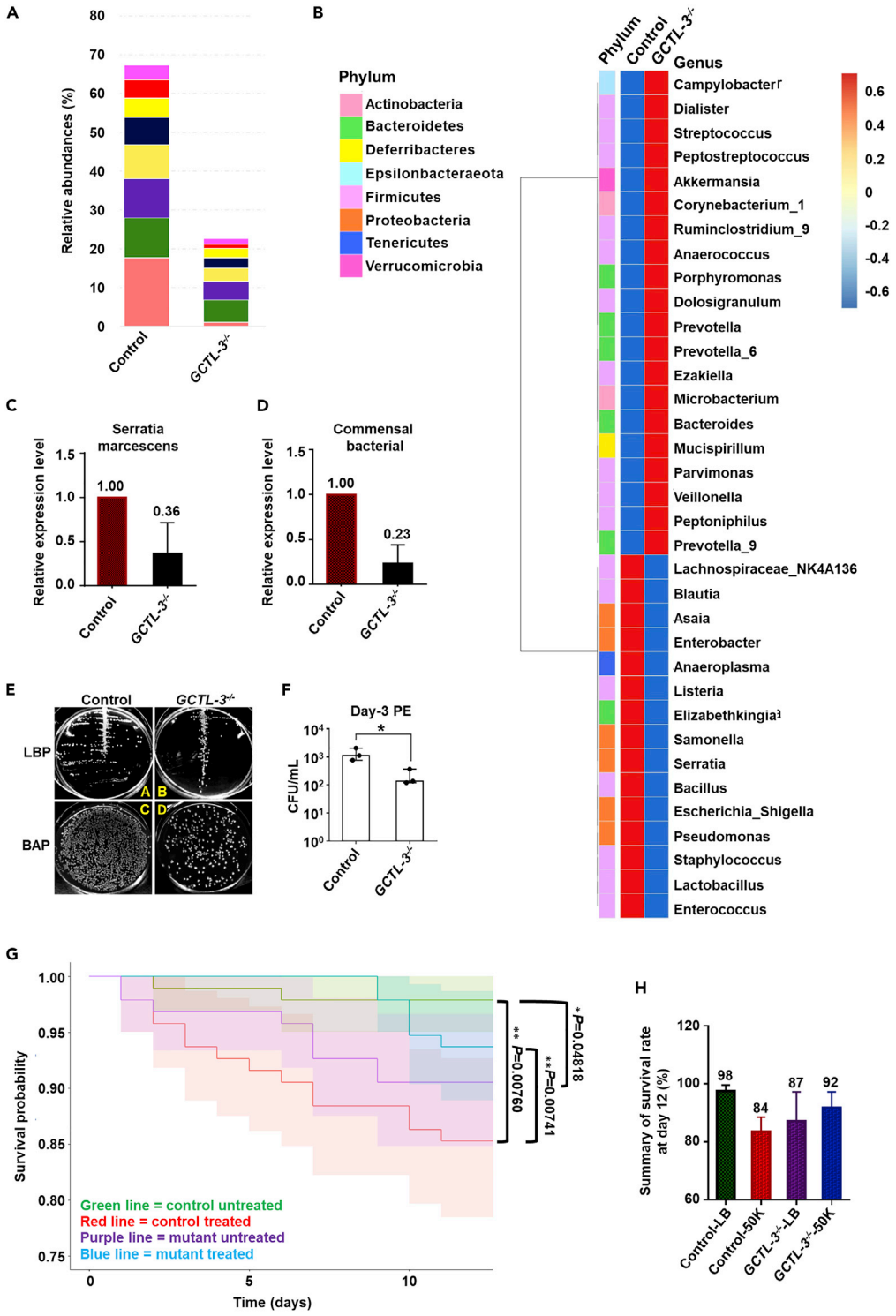

Figure 3. Reduced Colonization of *A. aegypti mosGCTL-3*$^{-/-}$ Midgut by Gut Bacteria

(A and B) 16S amplicon sequencing data from control and *GCTL-3*$^{-/-}$ mosquitoes. Sample sizes: all groups = 15.

(C and D) RT-PCR data indicated (C) commensal bacteria and (D) *S. mar* in *GCTL-3*$^{-/-}$ mosquitoes. Sample size: each group = 10; data are represented as mean ± SD.

Figure 3. *Continued*

(E and F) An abundance of bacteria detected in four mosquito whole bodies. *GCTL-3*$^{-/-}$ mosquitoes were found to have fewer bacteria than controls. Data are represented as median with interquartile range. Unpaired t test was applied; *p < 0.05.

(G) Mosquito survival curves following oral infection with *S. marcescens*; bacterial infection resulted in reduced mortality rates in mutants compared with controls. There were significant differences between genotypes (p = 0.0481) and treatment groups (p = 0.0076). The total sample size of each group was 95. Asterisks represent significant differences between the genotypes (Cox proportional hazards model; *p < 0.05, **p < 0.01). The solid line represents the median estimate, and the zones represent the confidence intervals, with the upper and lower bounds based on a Kaplan-Meier estimate.

(H) Summary of survival rate at day 12 following bacteria challenge. Data are represented as mean ± SD. 50K, treatment with 50,000 CFU/mL of *S. marcescens;* BAP, blood agar plate LB, lysogeny broth; LBP, lysogeny broth plate.

See also Table S5.

lectins became activated 1 to 3 days following a blood meal, including CTL-15, CTL-19, CTLGA-3, CTLGA-5, and GCTL-3 (Figure S1I, Supplemental Information, Table S6).

Before a blood meal, *GCTL-3*$^{-/-}$ mosquitoes showed elevated expression levels of *STAT* (AAEL009692) and *Vir-1* (AAEL000718), which are signaling components of the JAK/STAT pathway (Figure 4A, Supplemental Information, Table S7). Following a blood meal, however, these differences broadly disappeared, although *STAT* levels were still significantly greater in mutants 48 h post-blood meal. Taken together, these results suggest an activation of JAK/STAT signaling in *GCTL-3* mutants following blood meal consumption.

In addition, 48 h after a blood meal, *GCTL-3* knock-out also resulted in increased expression of *dredd* (AAEL014148) and *FADD* (AAEL001932), both of which are components of the IMD pathway (Figure 4B, Supplemental Information, Table S7). The uptake of a blood meal did not seem to affect regulation of either the Toll or RNAi pathway in *GCTL-3* mutants (Figures 4C and 4D, Supplemental Information, Table S7). However, blood meal provision resulted in significantly higher expression levels of *Attacin* (*ATT*, AAEL003389) and *Gambicin* (*GAM*, AAEL004522), but not *Defensin E* (*Def E*, AAEL000611), in mutants 48 h after the blood meal. All comparisons were analyzed using two-way ANOVA (Figure 4E, Supplemental Information, Table S7); full details of the ANOVA values related to Figure 4 are recorded in Supplemental Information Table S8.

Collectively, the data shows an elevated immuno-response in *GCTL-3* mutants compared with controls after consumption of a blood meal. A previous study by Ramirez et al. found that transcript abundance of mosquito AMP genes changed 2 days after mosquito midgut bacteria were introduced (Ramirez et al., 2012); this indicates that *GCTL-3* not only influences viral dynamics but also regulates gut homeostasis and innate immune response following blood meal uptake, suggesting that *GCTL-3* influences multiple *in vivo* functions.

GCTL-3 Knock-out Resulted in Defects in Mosquito Fertility and Fecundity

To better understand the relationship between immunity and reproduction, we next investigated the effect of upregulation of the JAK/STAT and AMPs pathway and altered gut microbiota populations arising from *GCTL-3* knock-out on mosquito fecundity and fertility. The numbers of embryos laid per female and egg hatching rate were both significantly reduced in *GCTL-3*$^{-/-}$ mosquitoes when compared with controls; female controls produced approximately 100 embryos each, around double that of mutants, whereas hatching rate was reduced from 90% to 40% in mutants (Mann-Whitney test; p < 0.0001 for both embryo number and hatched larvae; Transparent Methods; Figures 5A and 5B). *GCTL-3* knock-out also caused embryo melanization and abnormally shaped ovarioles in mutants (Supplemental Information, Figures S4A and S4B, Data S7); although melanization plays an important role in the invertebrate defense system, here it likely led to a significant increase in the number of non-viable eggs (Shin et al., 2011; Zou et al., 2010). We found that the *GCTL-3* knock-out caused defects in mosquito oviposition that were not PPO3-dependent (Supplemental Information, Figure S4C).

To address whether decreases in fecundity and fertility were due to defects in either male or female mosquitoes (or both), we back-crossed *GCTL-3*$^{-/-}$ male or female mosquitoes with wild-type mosquitoes. We found no differences between controls and *GCTL-3*$^{-/-}$ males in terms of fecundity (Mann-Whitney test; p = 0.5995; Figure 5C) but identified a significant reduction in *GCTL-3*$^{-/-}$ male fertility (Mann-Whitney test;

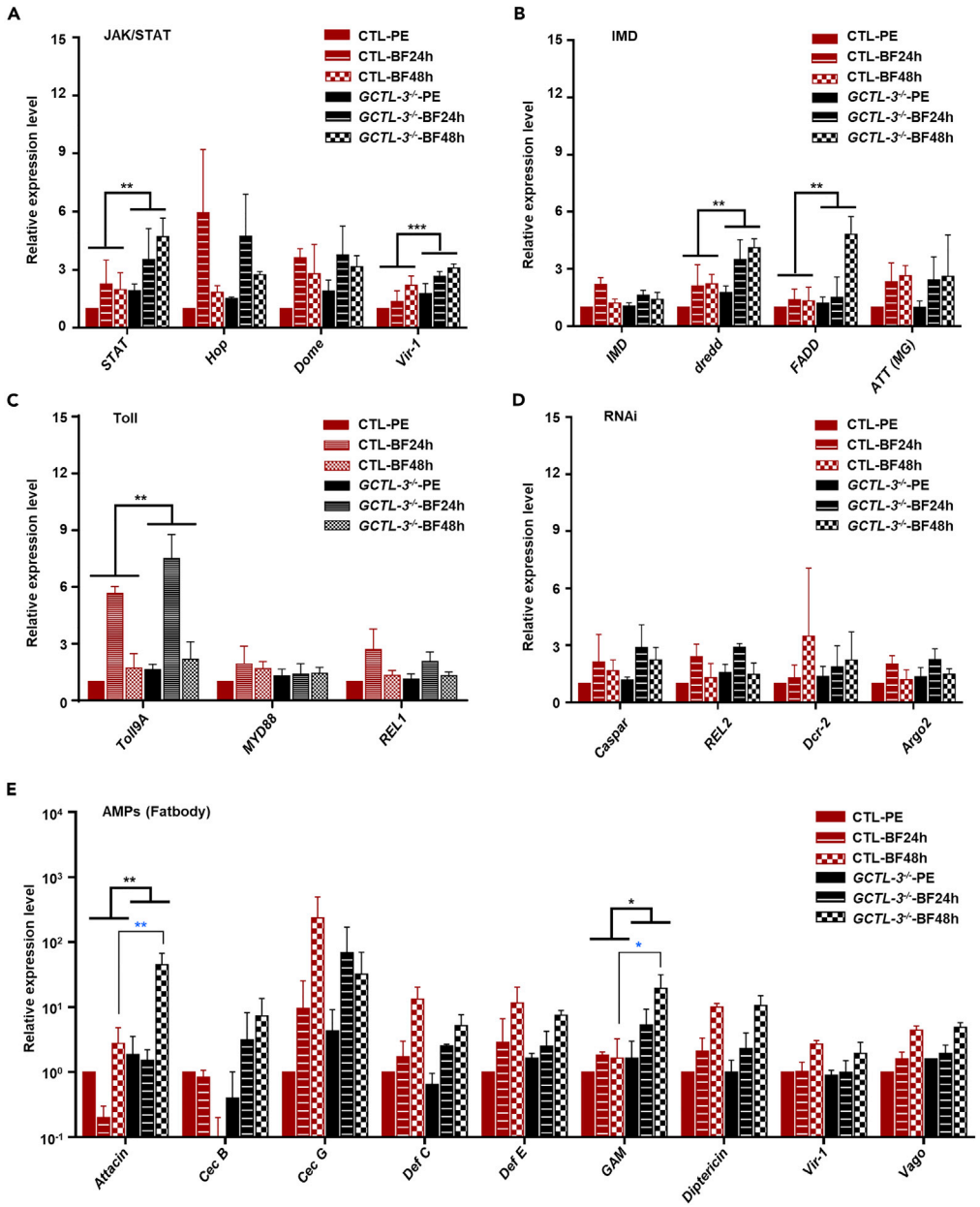

Figure 4. Knock-out of *GCTL-3* Causes a Change in the Regulation of JAK/STAT and AMP Signaling Pathway Genes

(A–E) Midguts and fat bodies were dissected and collected from 7-day-old control and *GCTL-3*$^{-/-}$ mosquitoes 24 and 48 h after blood feeding. Gene expression was normalized to the *A. aegypti* housekeeping gene RpS7. *GCTL-3*$^{-/-}$ mosquitoes showed higher expression levels at marked time points in the (A) JAK/STAT, (B) IMD, (C) Toll, (D) RNAi, and (E) AMPs pathways. Sample sizes: all groups = 10. Data are represented as mean ± SD. Black asterisks represent significant differences between the genotypes (two-way ANOVA; *$p < 0.05$, **$p < 0.01$, ***$p < 0.001$; exact p values for each comparison can be found in Supplemental Information, Table S7 and Data S2) and blue asterisks represent significant differences between genotypes at a particular time. BF, blood feed; PE, post-eclosion.
See also Tables S7 and S8.

$p < 0.0001$; Figure 5D), indicating that there may be a reduction in sperm count in mutant males. We further found that *GCTL-3*$^{-/-}$ females exhibited strong reductions both in fecundity and fertility, by counting the eggs of mosquitoes and the number of larvae hatched in next generation (fecundity of controls = 37; fecundity of mutants = 43; Mann-Whitney test; $p < 0.0001$; Figures 5E and 5F). We also checked for differences in

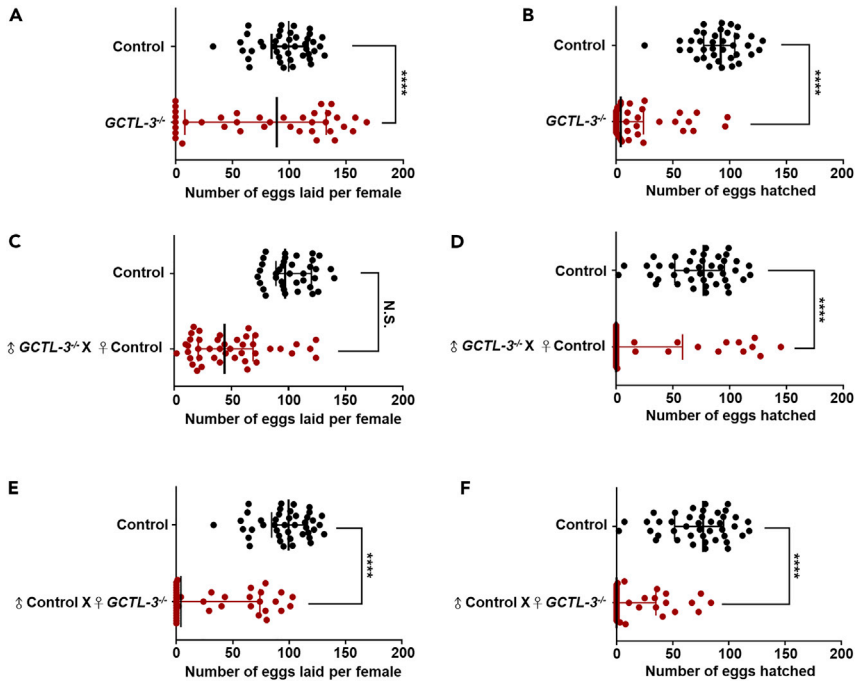

Figure 5. *GCTL-3*$^{-/-}$ Mutants Show Reduced Oviposition and Egg Hatch Rates Compared with Controls

(A and B) (A) Number of embryos and (B) number of hatched larvae for *mosGCTL-3*$^{-/-}$ mutants and controls. Sample sizes: control = 37; *GCTL-3*$^{-/-}$ = 43.

(C–F) (C and D) Mutant male (N = 38) and (E and F) female (N = 39) mosquitoes were backcrossed to control mosquitoes carrying mutations for *A. aegypti GCTL-3* genes, and the number of embryos and larvae in *GCTL-3*$^{-/-}$ mutant and control progeny in the subsequent generation were recorded. Sample sizes: control = 42; *GCTL-3*$^{-/-}$ = 42.

Data are represented as median with interquartile range. Asterisks represent significant differences between the genotypes (Mann-Whitney test; ****$p < 0.0001$. $p = 0.5995$ for (C); $p < 0.0001$ for (A, B, and D–F); Supplemental Information, Data S3).

physiology, which included body weight, body size, wing size, host-seeking behavior, and survival rates of mosquitoes and found that female mutant lifespan was significantly shorter than that of controls (Supplemental Information, Figure S5 and Data S8).

Germline Abnormalities in the Ovaries of *GCTL-3*$^{-/-}$ Mutants and the Loss of *GCTL-3* in the Mosquito Midgut Activated Apoptotic Signaling Pathways

To better understand the mechanisms underlying the reduced fertility of *GCTL-3*$^{-/-}$ mosquitoes, we examined mutant ovaries 4 days after a blood meal. *GCTL-3*$^{-/-}$ mosquitoes were found to have significantly fewer ovarioles than controls (Mann-Whitney test; $p = 0.0250$; Figures 6A and 6D), suggesting defects in early germ line development.

We therefore investigated germline development in control and *GCTL-3*$^{-/-}$ pupae via immunohistochemistry using an anti-*Aa*. VASA antibody. VASA is an evolutionarily conserved germ cell maker found in many different organisms (Castrillon et al., 2000; Gustafson and Wessel, 2010; Raz, 2000). VASA immunostaining also indicated a reduction of signal in *GCTL-3*$^{-/-}$ pupae gonads (Figure 6B right and 6E) and ovaries compared with controls (Figure 6B left). Furthermore, a significant fraction of blood-fed mutant ovarioles did not contain a germarium, the anterior region of the ovariole likely to contain germline stem cells (Figure 6C left and 6F), suggesting that *GCTL-3* contributes to mosquito germline development. We also observed increased expression of the apoptosis marker cleaved-caspase-3 in *GCTL-3*$^{-/-}$ ovaries (Supplemental Information, Figures S6A and S6C, Data S9). The reduction in germ cells and increased levels of apoptosis are thus likely the cause of the reduced number of eggs produced by mutant females. Similarly, many *GCTL-3*$^{-/-}$ testes were less organized and exhibited a reduced VASA signal (Figure 6C right and 6G, Data S9) as well as an increased cleaved-caspase-3 signal (Supplemental Information, Figures S6B and S6D,

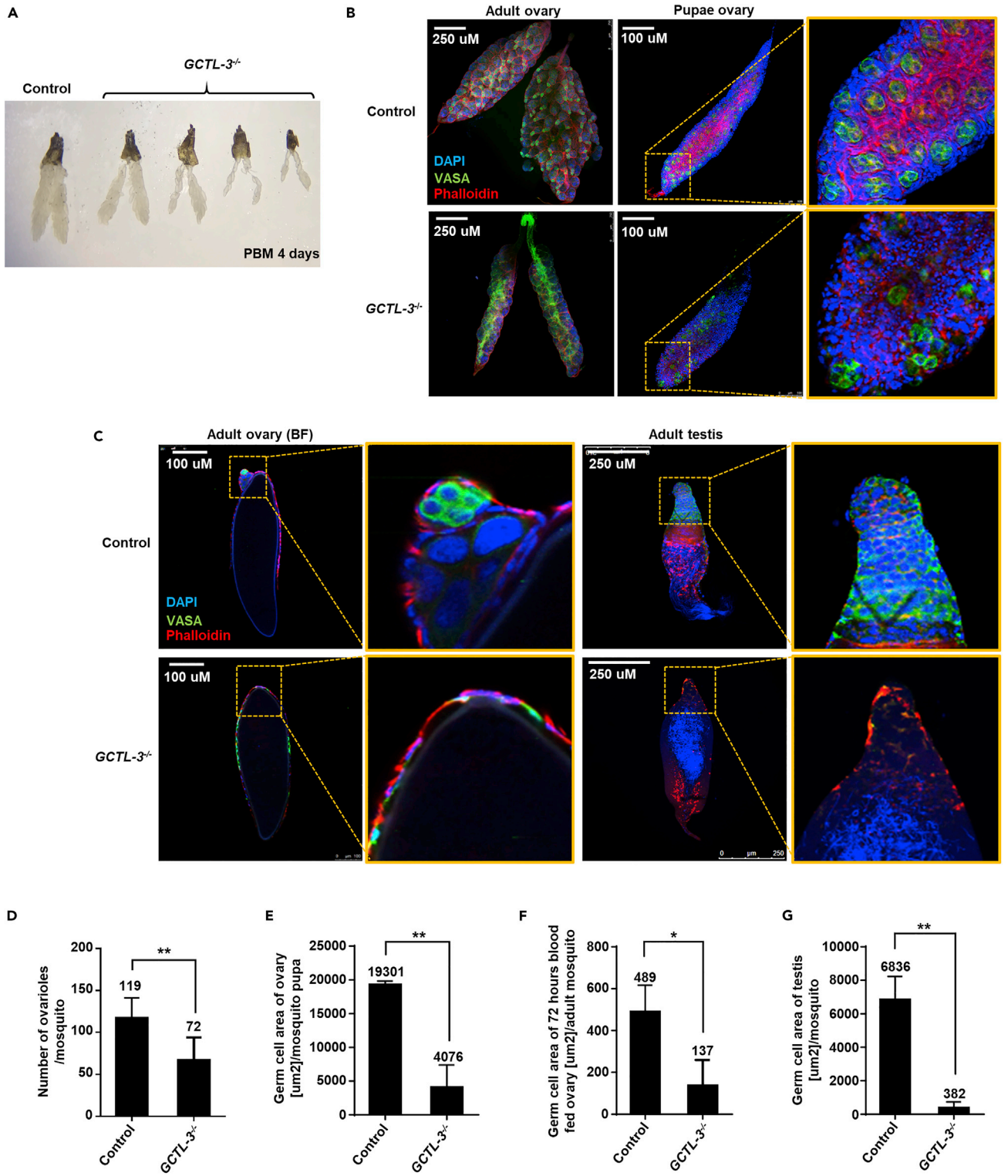

Figure 6. VASA Expression in *GCTL-3*$^{-/-}$ Ovaries

(A) Comparison of ovaries of 5- to 7-day-old control (left) and *GCTL-3*$^{-/-}$ (right) mosquitoes. Sample sizes: all groups = 7.

(B and C) VASA expression in 5- to 7-day-old control and *GCTL-3*$^{-/-}$ female (B) non-blood-fed adult and pupae ovaries as well as (C) 72-h post-blood-fed ovaries and adult male testes.

Figure 6. *Continued*

(D–G) Quantification of immunostaining across three samples in (D) non-blood-fed female ovaries, (E) pupae ovaries, (F) 72-h post-blood-fed ovaries, and (G) male testes. Anti-VASA was used as a primary antibody (1:500), and Alexa Fluor 488 dye was used as a secondary antibody (1:500) along with DAPI and phalloidin staining to mark the cell nuclei and cytoskeletons.

Data are represented as median with interquartile range. Stars represent significant differences between the genotypes (Mann-Whitney test; *$p < 0.05$, **$p < 0.01$. $p = 0.0089$ for (D); $p = 0.0014$ for (E); $p = 0.0262$ for (F); $p = 0.0015$ for (G); Supplemental Information, Data S4). BF, blood feed.

Data S9). Furthermore, some *GCTL-3*$^{-/-}$ testes were found to lack VASA-expressing germ cells (Figure 6B right and 6C, Data S9).

In addition to its role during early germline development, *GCTL-3* also seems to serve a vital function in regulating mosquito oogenesis. In control mosquitoes, germline stem cells/progenitors undergo three rounds of synchronized divisions to produce an 8-cell cyst (7 nurse cells and 1 oocyte) with three ring canals connecting the oocyte to the nurse cells, whereas the *Drosophila* germline stem cell undergoes four rounds of synchronized divisions to produce a 16-cell cyst (Spradling, 1993). However, 17.27% of *GCTL-3*$^{-/-}$ follicles analyzed contain a 16-cell cyst (0.95% in control), indicating four rounds of germline cell divisions. Consistent with one extra round of germline cell division in these follicles, these follicles contained 15 polypoid nurse cells and one oocyte (Figure 7A). Furthermore, the oocyte was connected to the nurse cells via four ring canals instead of the usual three ring canals found in a normal 8-cell follicle (not shown).

We found that *GCTL-3*$^{-/-}$ ovaries also exhibit defective encapsulation in terms of individualization of germline cysts. In control mosquito ovaries, each germline cyst is encapsulated by a layer of somatic cells upon exit of germarium to form a germline follicle. Each follicle is separated from neighboring follicles by a stack of interfollicle stalk cells. In *GCTL-3*$^{-/-}$ ovaries, however, 22.87% of follicles were identified as compound follicles, containing fused follicles with various germ cells and lacking interfollicle stalk cells (Supplemental Information, Table S9).

Previous reports indicated that during *Drosophila* oogenesis, defects in the Notch pathway can produce similar encapsulation defects (Ruohola et al., 1991; Xu et al., 1992). We therefore examined Notch localization in mosquito follicular cells. Similar to its localization in *Drosophila* follicular cells, Notch (recognized by an anti-*Drosophila* NICD antibody) was expressed and mainly localized on the apical domain (facing the germline side) of follicular cells in control mosquitoes. We found weak apical localization in *GCTL-3*$^{-/-}$ follicular cells (Figure 7B), suggesting that *GCTL-3* may play a role in regulating Notch apical localization, which may be the cause of the defective encapsulation. We also found that cleaved-caspase-3 signal accumulated in *GCTL-3*$^{-/-}$ midguts following a blood meal. This was clear from both qPCR (Supplemental Information, Figure S7A, Data S10) and immunostaining (Supplemental Information, Figure S7B) data and was not the case for control mosquitoes.

Attacin and *Gambicin* Knock-down Partially Rescued Reductions in *GCTL-3*$^{-/-}$ Fertility and Fecundity

Changes in expression levels of components of the AMPs immunological pathway have been found to significantly affect insect reproductive capabilities (Camaioni et al., 2018; Delhaye et al., 2016; Schwenke et al., 2016). Given the significant increase found for various elements of this pathway in *GCTL-3*$^{-/-}$ mutants (Figure 4E), we hypothesized that reducing the expression of these elements may rescue female fecundity. As lower doses of dsRNA (of 1μg) were not effective to knock-down AMPs in *GCTL-3*$^{-/-}$ mutants (data not shown), we instead used 1.5 μg dsRNA to knock-down *Attacin* and *Gambicin*, which we identified as significantly upregulated in mutants following a blood meal (Figure 4E), to assay the role of *GCTL-3* in the immunity to reproduction trade-offs.

dsATT and dsGAM injection does not affect control egg laying rate, but restores *GCTL-3*$^{-/-}$ mutant egg laying rate to control levels (two-way ANOVA; $p < 0.05$ respectively; Figures 8C and 8D left, Supplemental Information, Tables S10 and S11). dsATT and dsGAM injections do not, however, restore *GCTL-3*$^{-/-}$ mutant larval hatching to control levels, although they still significantly increase the number of larvae hatching compared with control and dsLacZ injections (two-way ANOVA; $p < 0.05$ for all comparisons). No differences were found between any control groups (two-way ANOVA; $p > 0.05$) (Figures 8C and 8D right, Supplemental Information, Tables S10 and S11).

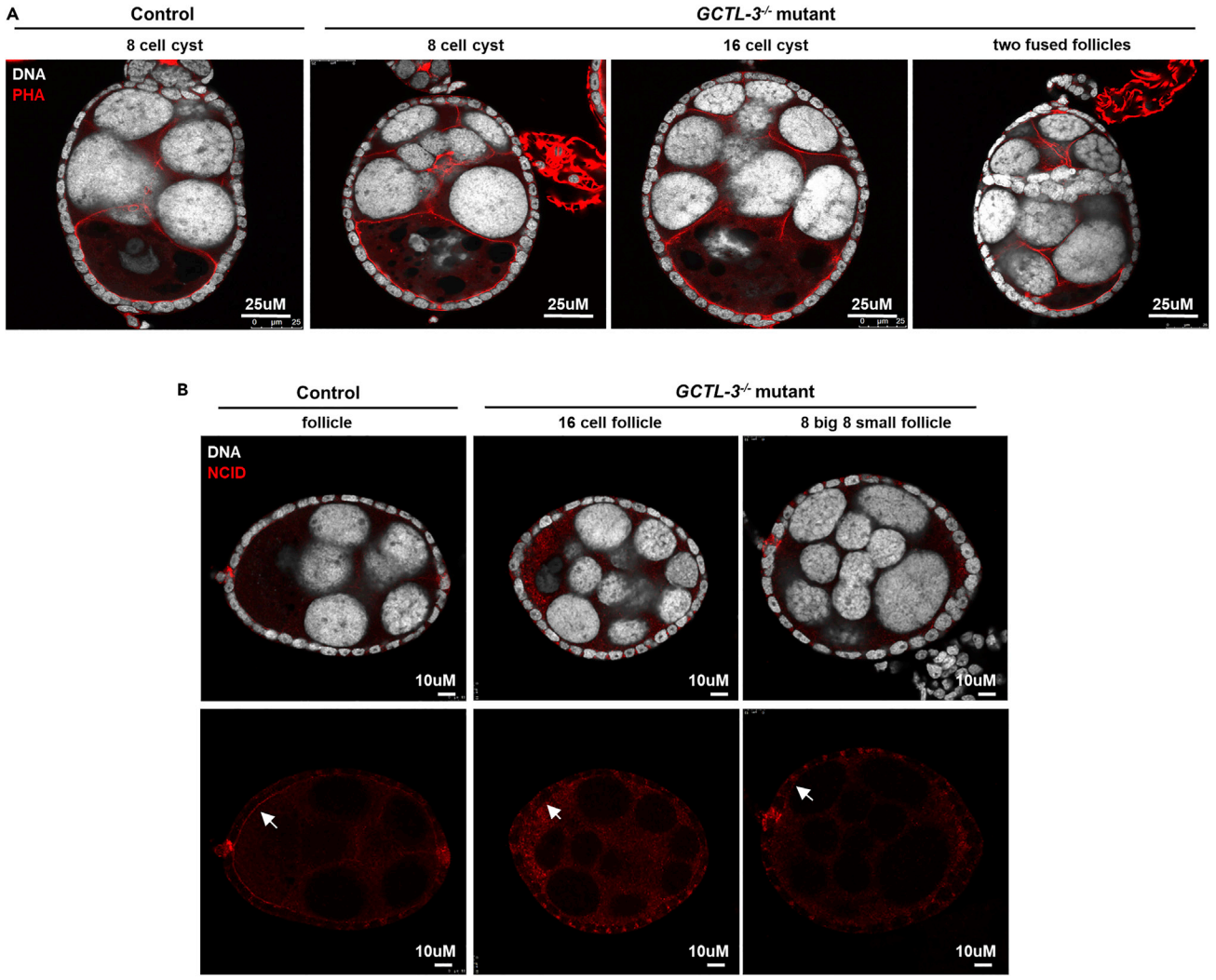

Figure 7. Defects in *GCTL-3*$^{-/-}$ Follicles

(A) Left, a control follicle containing seven nurse cells and one oocyte; right, a *GCTL-3*$^{-/-}$ follicle containing various numbers of nurse cells and oocytes.

(B) NICD (labeled by arrows) is mainly localized on the apical side of follicular cells in control mosquitoes (left); the extent of this localization is reduced in *GCTL-3*$^{-/-}$ follicular cells. DNA was visualized using Hoechst staining.

See also Table S9.

DISCUSSION

Recent years have seen major breakthroughs in mosquito gene editing techniques, ranging from the initial demonstration of CRISPR/Cas9 in *A. aegypti* to the knock-out of kynurenine hydroxylase (*kh*) and dopachrome conversion enzyme (*yellow*), thus creating mosquito white eye (loss of pigment) and yellow body mutants, to the establishment of transgenic germline-specific Cas9 *A. aegypti* founder strains (Kistler et al., 2015; Li et al., 2017; Liu et al., 2018; Yang et al., 2019). Basu et al. and Li et al. previously used the CRISPR-Cas9 system to generate site-specific mutations in *A. aegypti* by injecting *in vitro*-transcribed sgRNA that used a homology-directed repair (HDR) technique. Here, we used the *Aedes* U6 promoter to drive sgRNA expression *in vivo* and co-injected the U6 promoter-driven sgRNA template with the HDR construct plasmid.

By applying this methodology, we were able to knock-out a member of the CTL family, *GCTL-3*, to investigate the resource trade-offs that occur in female mosquitoes following pathogen infection. Previous mosquito work on reproductive/immunological trade-offs has mainly focused on *Anopheles gambiae*. CRISPR/Cas9 methodologies have been used in that study to generate a mosaic gamma-interferon-inducible

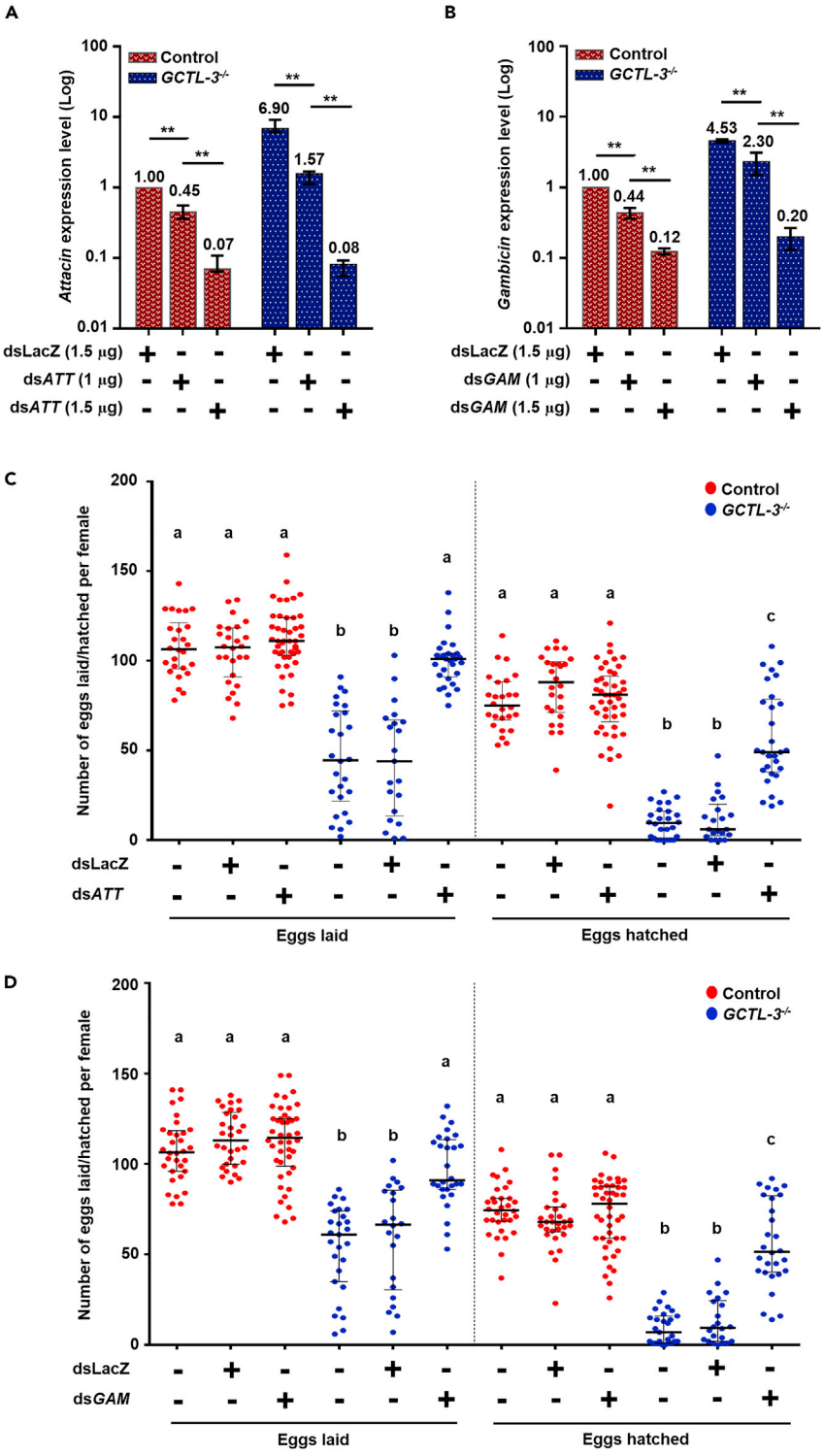

Figure 8. Attacin and Gambicin Knock-down Partially Rescued Reductions in *GCTL-3*$^{-/-}$ Fertility and Fecundity

(A and B) Change in (A) *Attacin* and (B) *Gambicin* expression levels for control and *GCTL-3*$^{-/-}$ mosquitoes at different time points and injection states detected via reverse transcription-PCR. Data are represented as mean ± SD. (N = 6 for each group. Mann-Whitney test; **p < 0.01).

(C and D) Egg (left) and larval hatch (right) counts for control (red) and *GCTL-3*$^{-/-}$ (blue) mutants following no injection, dsLacZ injection, dsATT injection and dsGAM injection. Each point represents an egg/larval hatch count for an individual

Figure 8. *Continued*

female. Sample sizes for *Attacin* testing: Control = 26; Control + dsLacZ = 26; Control + dsATT = 45; *GCTL-3*$^{-/-}$ = 21; *GCTL-3*$^{-/-}$ + dsLacZ = 26; *GCTL-3*$^{-/-}$ + dsATT = 29. Sample sizes for *Gambicin* testing: Control = 32; Control + dsLacZ = 30; Control + dsGAM = 44; *GCTL-3*$^{-/-}$ = 27; *GCTL-3*$^{-/-}$ + dsLacZ = 22; *GCTL-3*$^{-/-}$ + dsGAM = 28. dsLacZ/dsATT/dsGAM represents groups injected with double-stranded RNA for LacZ/*Attacin*/*Gambicin*.

Data are represented as median with interquartile range. Different letters represent significant differences between groups (two-way ANOVA; adjusted $p < 0.05$). Exact p values for each comparison can be found in Supplemental Information, Table S11 and Data S5.

See also Tables S10 and S11.

lysosomal thiol reductase (mos*GILT*) mutant line, which showed both defects in ovary development and an anti-*Plasmodium* phenotype (Yang et al., 2019). No such mutants have previously been generated in *A. aegypti*, however, and only the general mechanisms underlying these trade-offs are known.

We confirmed that AAEL000535 was a member of the CTL family based both on previous work on *A. aegypti* CTL and a recent article by Pascini et al., who provided information regarding the reassembled coding sequences of AAEL000535 and AAEL029058 (Pascini et al., 2020). This information indicated that in terms of DNA/RNA sequences, AAEL000535 and AAEL029058 are the same locus and belong to the CTLs. Based on a Vectorbase alignment of the sequences, we believe AAEL000535 may either be the same gene or an alternative splicing form of AAEL029058 that lacks the additional putative sequence on the N-terminal region of the protein.

Prior publications have discussed the role played by various signaling pathways, including the Toll, IMD, JAK-STAT, and RNAi pathways, in limiting pathogen propagation following infection (Kumar et al., 2018). Mosquito commensal microbiota also play a vital role in DENV immunological responses via activation of the Toll immune pathway, whereas increased expression of JAK-STAT signaling components in the mosquito fat body has been shown to inhibit DENV infection in the midgut and the salivary glands (Jupatanakul et al., 2017; Xi et al., 2008). Moreover, each mosquito tissue performs specific antiviral strategies (Cheng et al., 2016). Each of these mechanisms is likely to lead to a reduction in mosquito reproductive capabilities due to resource limitations. CTLDcps expression level varies significantly between males and females, as well as across different developmental stages and parts of the mosquito body (Adelman and Myles, 2018). We thus investigated expression levels of *GCTL-3* in different male and female *A. aegypti* body parts, including the head, thorax, fat body, ovary, and testis. Expression levels in the head were found to be higher than in any other body part for both sexes (Supplemental Information, Figures S1G and S1H), suggesting that *GCTL-3* may play a role in regulating brain function.

DENV-2 (NGC strain) has been reported to be particularly virulent and the cause of many severe dengue outbreaks (Wang et al., 2016; Williams et al., 2014; Yung et al., 2015). Most research articles (Molina-Cruz et al., 2005; Salazar et al., 2007; Sanchez-Vargas et al., 2018; Sri-In et al., 2019; Tree et al., 2019) have used DENV-2 for proof-of-principle experiments. Here we utilized DENV-2 NGC, the most commonly used strain. In this study, we found that *GCTL-3*$^{-/-}$ *A. aegypti* mutants showed a reduction in DENV-2 infection rate and altered expression levels for various components of key signaling pathways, indicating that *GCTL-3* is involved in the JAK-STAT, IMD, Toll pathways, and AMPs activation. In the previous article by Liu et al. (2014), RNAi knock-down of *GCTL-3* decreased DENV replication; here, however, knock-out of *GCTL-3* did not lead to a reduction in virus titer. A median decrease in viral titer of 60% could have a significant effect on the resulting infection rate (Buchman et al., 2019; Souza-Neto et al., 2019); verification of *GCTL-3* mutant infection rates is therefore a necessary next step.

Following a blood meal, the JAK-STAT pathway became activated and downstream AMPs expression levels were altered. We found that *GCTL-3* knock-out led to a reduction in the number of gut microbiota, suggesting that *GCTL-3* plays a role in promoting gut microbiota homeostasis. This may be related to significant increases in expression levels seen for two AMPs, *Gambicin* and *Attacin*, in *GCTL-3*$^{-/-}$ mutants. The regulation sites of the *Gambicin* promoter region have been identified, and *Gambicin* can be induced by the IMD, Toll, and JAK-STAT pathways via combinatorial regulation in *A. aegypti* Aag2 cells (Zhang et al., 2017). Furthermore, *Attacin* has been reported to combat Gram-negative bacterial infection in *Drosophila* (Wicker et al., 1990).

Mosquitoes are hematophagous insects that can obtain many pathogens via blood feeding; the first line of defense to these pathogens is therefore the intestinal tract, which includes the gut commensal microbiome. This microbiome can be highly diverse, with 21 bacterial species having been identified in the

A. aegypti Rockefeller strain (Wu et al., 2019). From our 16S sequencing data and CFU assay results, it is clear that *GCTL-3* knock-out causes a change in gut bacteria homeostasis. This is particularly relevant in the case of *S. marcescens*, which has been identified as the main bacterium in control mosquito midguts and can enhance viral dissemination in mosquitoes (Wu et al., 2019). In our study, loss of *GCTL-3* resulted in a corresponding loss of *S. marcescens* from the mosquito midgut, which may be the cause of the decreased virus infection rate found in mutants. Formation of a microbiota-induced peritrophic matrix has previously been reported as preventing pathogen infection via regulation of midgut homeostasis in *Anopheles* mosquitoes (Rodgers et al., 2017). Further research into expression levels of *Sm*Enhancin and structure formation of the peritrophic matrix in *A. aegypti* is thus of great interest.

Gut homeostasis plays an important role in determining developmental rate and reproductive output in many species (Elgart et al., 2016; Leitao-Goncalves et al., 2017). Correspondingly we found that *GCTL-3* mutants, whose gut microbiota populations were severely reduced compared with controls, exhibited clearly defective ovaries and testes as well as shortened lifespans. We also noticed defects in germline development; in controls, 93.3% of germline follicles were normal (i.e., contained seven nurse cells and one oocyte [total = 393]), whereas only 50.6% of germline follicles were found to be normal in *GCTL-3* female mutants (total = 411) (Supplemental Information, Table S9). Knock-out of *GCTL-3* in *A. aegypti* thus appears to cause similar germline developmental defects as removal of the gut bacteria of *Drosophila*. CTLs thus play an important role in germ line development and reproduction.

Uptake of a blood meal by a female mosquito results in the production of two signals: a direct signal to the fat body, activated by yolk protein precursor (YPP) gene expression, and an indirect signal from the midgut to the brain. The latter signal activates medial neurosecretory cells to release a peptide hormone, ovarian ecdysteroidogenic hormone (OEH), which then produces ecdysone in the fat body to activate the steroid hormone, 20-hydroxyecdysone (20E). 20E in turn activates YPP gene expression (Raikhel et al., 2005). In this study, the highest levels of *GCTL-3* mRNA were found in the mosquito head, suggestive of a role for *GCTL-3* in modulating brain function.

Production of AMPs has been found to alter female mosquito response to pathogens (Schwenke et al., 2016). Here we used dsRNA to knock-down two components of the AMPs pathway, *Attacin* and *Gambicin*, which were found to be significantly upregulated in mutants compared with controls following consumption of a blood meal. We found that suppression of *Attacin* and *Gambicin* could rescue in part the reproductive defects of mutants, implying that *Attacin* and *Gambicin* may play important roles in *GCTL-3*-mediated reproductive processes.

Silencing of *AaNotch* and *AaJNK* results in significant reductions of female mosquito fecundity and fertility (Chang et al., 2018). Our data indicate a reduction in Notch signal intensity or alterations in localization in *GCTL-3* mutant ovaries 24 h post-blood meal, implying that CTLs may influence Notch localization and activity during reproductive processes.

Activation of apoptosis is a hallmark of host cell protection against pathogenic infection; this is executed by the family of cysteinyl proteases that includes caspase 3, whose activation is a crucial event for efficient influenza virus propagation (Thornberry and Lazebnik, 1998; Wurzer et al., 2003). Previous reports have indicated that the denudation of germline development is sufficient to extend the lifespan in *C. elegans* and *Drosophila* (Flatt et al., 2008; Yunger et al., 2017). In mosquitoes, the role of *GCTL-3* in affecting longevity is not clear. Here, we used a cleaved-caspase-3 antibody to address germline defects in *GCTL-3* mutants and identified up-regulated apoptotic signals. This could thus result in ovary defects and inhibit viral load in the mosquito midgut. *Michelob_x* (*Mx*) and *IMP*, two IAP antagonists involved in the apoptosis pathway, act on both initiator and effector caspases (Wang and Clem, 2011). Our data showed that loss of *GCTL-3* also resulted in caspase-3 activation after a blood meal, suggesting that *GCTL-3* may either introduce DIAP1 to the midgut or bind with *Mx* and/or *IMP* to protect *DIAP1* from degradation. Either mechanism would result in inhibition of apoptosis in the mosquito midgut.

Loss of *GCTL-3* caused activation of the genes *Hop*, *Dome*, and *STAT*, all of which play a role in the JAK-STAT pathway post-eclosion, as well as activation of the downstream gene *Vir-1* 24 48 h after a blood meal. Knock-out of *GCTL-3* also activated the IMD pathway, which represents another innate immunity defense mechanism. In *Drosophila*, the FADD (DmFADD) and caspase-8 homologs (DREDD) can associate with IMD

to form a multimeric complex (Georgel et al., 2001). Here we found that post-eclosion and 48 h post-blood meal FADD and DREDD, in addition to *Attacin*, *Gambicin*, and *Defencin E*, were also activated in *GCTL-3*$^{-/-}$ mutant mosquitoes. This pathway may also lead to upregulation of apoptosis markers and block DENV and ZIKV infections.

Finally, whereas many insect studies have identified negative correlations between up/down-regulation of immunological and reproductive pathways, few have determined the mechanisms, or components of these mechanisms, which modulate resource distribution (McKean et al., 2008). In *Drosophila melanogaster*, up-regulation of IMD and JNK signaling has been reported to downregulate insulin-like growth factor signaling and thus egg production; 20-hydroxyecdysone and juvenile hormone are also thought to be involved in this pathway (DiAngelo et al., 2009; Schwenke et al., 2016). Here, we found increased expression levels of several components of both signaling pathways, suggesting that this pathway may be conserved in *A. aegypti*. Generation of further knock-out mutants for other members of the lectin family could help to precisely identify the role they play in influencing the balance between reproductive and immunological systems.

In summary, we here established a mutant *A. aegypti* line and investigated the important relationship between CTLs and arbovirus infection. The observed reductions in virus infection rate are likely the result of changes in the gut microbiome, providing further evidence to the key role played by microbiota in infection rate within the mosquito itself. CTLs not only play a vital role in mosquito immune responses and gut homeostasis but also seem to have important functions in germline development and life span determination. A better understanding of the links between reproduction and immune response as mediated via the lectin family should provide new information regarding insect resource allocation processes.

Limitations of the Study

Based on our alignment, we believe that AAEL000535 is the truncated form of AAEL029058 lacking the N terminal. According to Vectorbase, AAEL029058 has an additional putative sequence on the N-terminal region of the protein belonging to the coding sequence. Given that the start codon is usually ATG (Methionine) for eukaryotic coding sequences, and that alternate start (non-ATG) codons are highly rare in eukaryotic genomes, there is insufficient evidence currently available to clarify which is the correct start codon for AAEL029058. Clarifying the full-length sequence of this gene is therefore important for validation purposes. Furthermore, testing whether the reduction in viral titer leads to a decrease in viral transmission rate would also provide valuable additional information.

Resource Availability

Lead Contact

Further information and requests for resources and reagents should be directed to and will be fulfilled by the Lead Contact, Chun-Hong Chen (chunhong@gmail.com).

Materials Availability

Materials generated in this study are available from the Lead Contact with a completed Materials Transfer Agreement.

Data and Code Availability

The published article includes all data generated or analyzed during this study.

METHODS

All methods can be found in the accompanying Transparent Methods supplemental file.

SUPPLEMENTAL INFORMATION

Supplemental Information can be found online at https://doi.org/10.1016/j.isci.2020.101486.

ACKNOWLEDGMENTS

We thank Cheng-Yu Liu for assistance with mosquito work; Tsai-Ling Yang and Jui-Fen Lai for assistance with bacteria work; Zou Zhen's lab for providing the PPO3 antibody; Goh Feng Guan for generating the anti-VASA antibody; and Pei-Sheng Lin and Li-Wei Chen for data analysis. We would like to thank Uni-

edit (www.uni-edit.net) for editing and proofreading this manuscript. This study was supported by the NHRI (National Health Research Institutes, Taiwan; grant no. NHRI-08A1-MRGP12-035 and NHRI-09A1-MRGP12-035) to C.-H.C. and Temasek Life Sciences Laboratory and Singapore Millennium Foundation to Y.C. H.-H.L. carried out her thesis research under the auspices of the Graduate Program of Biotechnology in Medicine, National Tsing Hua University, and National Health Research Institutes.

AUTHOR CONTRIBUTIONS

Conceptualization, H.-H.L., J.-C.L., and C.-H.C.; Methodology, H.-H.L. and J.-C.L.; Investigation, H.-H.L., Y.C., J.-C.L., S.-J.C., W.-L.L., and L.C.; Formal Analysis, H.-H.L. and M.P.S.; Resources, C.-H.C., Y.C., and G.-Y.Y.; Data Curation, H.-H.L.; Writing – Original Draft, H.-H.L. and M.P.S.; Writing – Review & Editing, H.-H.L., J.-C.L., M.P.S., Y.C., W.-L.L., H.-D.W., and C.-H.C.; Supervision, C.-H.C.; Project Administration, C.-H.C.; Funding Acquisition, C.-H.C.

DECLARATION OF INTERESTS

The authors declare no competing interests.

Received: December 11, 2019
Revised: April 14, 2020
Accepted: August 18, 2020
Published: September 25, 2020

REFERENCES

Adelman, Z.N., and Myles, K.M. (2018). The C-type lectin domain gene family in Aedes aegypti and their role in arbovirus infection. Viruses *10*, 367.

Anglero-Rodriguez, Y.I., MacLeod, H.J., Kang, S., Carlson, J.S., Jupatanakul, N., and Dimopoulos, G. (2017). Aedes aegypti molecular responses to zika virus: modulation of infection by the toll and Jak/stat immune pathways and virus host factors. Front. Microbiol. *8*, 2050.

Bertani, G. (2004). Lysogeny at mid-twentieth century: P1, P2, and other experimental systems. J. Bacteriol. *186*, 595–600.

Buchman, A., Gamez, S., Li, M., Antoshechkin, I., Li, H.H., Wang, H.W., Chen, C.H., Klein, M.J., Duchemin, J.B., Paradkar, P.N., et al. (2019). Engineered resistance to Zika virus in transgenic Aedes aegypti expressing a polycistronic cluster of synthetic small RNAs. Proc. Natl. Acad. Sci. U S A *116*, 3656–3661.

Camaioni, A., Klinger, F.G., Campagnolo, L., and Salustri, A. (2018). The influence of pentraxin 3 on the ovarian function and its impact on fertility. Front. Immunol. *9*, 2808.

Castrillon, D.H., Quade, B.J., Wang, T.Y., Quigley, C., and Crum, C.P. (2000). The human VASA gene is specifically expressed in the germ cell lineage. Proc. Natl. Acad. Sci. U S A *97*, 9585–9590.

Chang, C.H., Liu, Y.T., Weng, S.C., Chen, I.Y., Tsao, P.N., and Shiao, S.H. (2018). The non-canonical Notch signaling is essential for the control of fertility in Aedes aegypti. PLoS Negl. Trop. Dis. *12*, e0006307.

Cheng, G., Cox, J., Wang, P., Krishnan, M.N., Dai, J., Qian, F., Anderson, J.F., and Fikrig, E. (2010). A C-type lectin collaborates with a CD45 phosphatase homolog to facilitate West Nile virus infection of mosquitoes. Cell *142*, 714–725.

Cheng, G., Liu, Y., Wang, P., and Xiao, X. (2016). Mosquito defense strategies against viral infection. Trends Parasitol. *32*, 177–186.

Dambuza, I.M., and Brown, G.D. (2015). C-type lectins in immunity: recent developments. Curr. Opin. Immunol. *32*, 21–27.

Delhaye, J., Aletti, C., Glaizot, O., and Christe, P. (2016). Exposure of the mosquito vector Culex pipiens to the malaria parasite Plasmodium relictum: effect of infected blood intake on immune and antioxidant defences, fecundity and survival. Parasit. Vectors *9*, 616.

DiAngelo, J.R., Bland, M.L., Bambina, S., Cherry, S., and Birnbaum, M.J. (2009). The immune response attenuates growth and nutrient storage in Drosophila by reducing insulin signaling. Proc. Natl. Acad. Sci. U S A *106*, 20853–20858.

Elgart, M., Stern, S., Salton, O., Gnainsky, Y., Heifetz, Y., and Soen, Y. (2016). Impact of gut microbiota on the fly's germ line. Nat. Commun. *7*, 11280.

Flatt, T., and Kawecki, T.J. (2007). Juvenile hormone as a regulator of the trade-off between reproduction and life span in Drosophila melanogaster. Evolution *61*, 1980–1991.

Flatt, T., Min, K.J., D'Alterio, C., Villa-Cuesta, E., Cumbers, J., Lehmann, R., Jones, D.L., and Tatar, M. (2008). Drosophila germ-line modulation of insulin signaling and lifespan. Proc. Natl. Acad. Sci. U S A *105*, 6368–6373.

Fontes-Garfias, C.R., Shan, C., Luo, H., Muruato, A.E., Medeiros, D.B.A., Mays, E., Xie, X., Zou, J., Roundy, C.M., Wakamiya, M., et al. (2017). Functional analysis of glycosylation of zika virus envelope protein. Cell Rep. *21*, 1180–1190.

Georgel, P., Naitza, S., Kappler, C., Ferrandon, D., Zachary, D., Swimmer, C., Kopczynski, C., Duyk, G., Reichhart, J.M., and Hoffmann, J.A. (2001). Drosophila immune deficiency (IMD) is a death domain protein that activates antibacterial defense and can promote apoptosis. Dev. Cell *1*, 503–514.

Grimont, P.A., and Grimont, F. (1978). The genus Serratia. Annu. Rev. Microbiol. *32*, 221–248.

Gustafson, E.A., and Wessel, G.M. (2010). Vasa genes: emerging roles in the germ line and in multipotent cells. Bioessays *32*, 626–637.

Guzman, A., and Isturiz, R.E. (2010). Update on the global spread of dengue. Int. J. Antimicrob. Agents *36*, S40–S42.

Hurd, H. (2002). The costs of mounting an immune response are reflected in the reproductive fitness of the mosquito Anopheles gambiae. Oikos *97*, 371–377.

Johansson, M.A., Mier-y-Teran-Romero, L., Reefhuis, J., Gilboa, S.M., and Hills, S.L. (2016). Zika and the risk of microcephaly. N. Engl. J. Med. *375*, 1–4.

Jupatanakul, N., Sim, S., Anglero-Rodriguez, Y.I., Souza-Neto, J., Das, S., Poti, K.E., Rossi, S.L., Bergren, N., Vasilakis, N., and Dimopoulos, G. (2017). Engineered Aedes aegypti JAK/STAT pathway-mediated immunity to dengue virus. PLoS Negl. Trop. Dis. *11*, e0005187.

Kingsolver, M.B., Huang, Z., and Hardy, R.W. (2013). Insect antiviral innate immunity: pathways, effectors, and connections. J. Mol. Biol. *425*, 4921–4936.

Kistler, K.E., Vosshall, L.B., and Matthews, B.J. (2015). Genome engineering with CRISPR-Cas9 in the mosquito Aedes aegypti. Cell Rep. *11*, 51–60.

Kumar, A., Srivastava, P., Sirisena, P., Dubey, S.K., Kumar, R., Shrinet, J., and Sunil, S. (2018). Mosquito innate immunity. Insects *9*, 95.

Kurz, C.L., Chauvet, S., Andres, E., Aurouze, M., Vallet, I., Michel, G.P., Uh, M., Celli, J., Filloux, A., De Bentzmann, S., et al. (2003). Virulence factors of the human opportunistic pathogen Serratia marcescens identified by in vivo screening. EMBO J. *22*, 1451–1460.

Leitao-Goncalves, R., Carvalho-Santos, Z., Francisco, A.P., Fioreze, G.T., Anjos, M., Baltazar, C., Elias, A.P., Itskov, P.M., Piper, M.D.W., and Ribeiro, C. (2017). Commensal bacteria and essential amino acids control food choice behavior and reproduction. PLoS Biol. *15*, e2000862.

Li, M., Bui, M., Yang, T., Bowman, C.S., White, B.J., and Akbari, O.S. (2017). Germline Cas9 expression yields highly efficient genome engineering in a major worldwide disease vector, Aedes aegypti. Proc. Natl. Acad. Sci. U S A *114*, E10540–E10549.

Liu, L., Dai, J., Zhao, Y.O., Narasimhan, S., Yang, Y., Zhang, L., and Fikrig, E. (2012). Ixodes scapularis JAK-STAT pathway regulates tick antimicrobial peptides, thereby controlling the agent of human granulocytic anaplasmosis. J. Infect. Dis. *206*, 1233–1241.

Liu, Y., Zhang, F., Liu, J., Xiao, X., Zhang, S., Qin, C., Xiang, Y., Wang, P., and Cheng, G. (2014). Transmission-blocking antibodies against mosquito C-type lectins for dengue prevention. PLoS Pathog. *10*, e1003931.

Liu, K., Qian, Y., Jung, Y.S., Zhou, B., Cao, R., Shen, T., Shao, D., Wei, J., Ma, Z., Chen, P., et al. (2017). mosGCTL-7, a C-type lectin protein, mediates Japanese encephalitis virus infection in mosquitoes. J. Virol. *91*, e01348-16.

Liu, T., Yang, W.Q., Xie, Y.G., Liu, P.W., Xie, L.H., Lin, F., Li, C.Y., Gu, J.B., Wu, K., Yan, G.Y., et al. (2018). Construction of an efficient genomic editing system with CRISPR/Cas9 in the vector mosquito Aedes albopictus. Insect Sci. *26*, 1045–1054.

McKean, K.A., Yourth, C.P., Lazzaro, B.P., and Clark, A.G. (2008). The evolutionary costs of immunological maintenance and deployment. BMC Evol. Biol. *8*, 76.

Miyashita, A., Lee, T.Y.M., McMillan, L.E., Easy, R., and Adamo, S.A. (2019). Immunity for nothing and the eggs for free: apparent lack of both physiological trade-offs and terminal reproductive investment in female crickets (Gryllus texensis). PLoS One *14*, e0209957.

Molina-Cruz, A., Gupta, L., Richardson, J., Bennett, K., Black, W.t., Barillas-Mury, C., et al. (2005). Effect of mosquito midgut trypsin activity on dengue-2 virus infection and dissemination in *Aedes aegypti*. Am. J. Trop. Med. Hyg. *72*, 631–637.

Pang, X., Xiao, X., Liu, Y., Zhang, R., Liu, J., Liu, Q., Wang, P., and Cheng, G. (2016). Mosquito C-type lectins maintain gut microbiome homeostasis. Nat. Microbiol. *1*, 16023.

Pascini, T.V., Ramalho-Ortigão, M., Ribeiro, J.M., Jacobs-Lorena, M., Martins, G.F., et al. (2020). Transcriptional profiling and physiological roles of *Aedes aegypti* spermathecal-related genes. BMC Genomics *21*, 143.

Patil, C.D., Patil, S.V., Salunke, B.K., and Salunkhe, R.B. (2011). Prodigiosin produced by Serratia marcescens NMCC46 as a mosquito larvicidal agent against Aedes aegypti and Anopheles stephensi. Parasitol. Res. *109*, 1179–1187.

Raikhel, A.S., Brown, M.R., Belles, X., et al. (2005). Hormonal Control of Reproductive Processes (Elsevier BV), pp. 433–491.

Ramirez, J.L., Souza-Neto, J., Torres Cosme, R., Rovira, J., Ortiz, A., Pascale, J.M., and Dimopoulos, G. (2012). Reciprocal tripartite interactions between the Aedes aegypti midgut microbiota, innate immune system and dengue virus influences vector competence. PLoS Negl. Trop. Dis. *6*, e1561.

Raz, E. (2000). The function and regulation of vasa-like genes in germ-cell development. Genome Biol. *1*, REVIEWS1017.

Rodgers, F.H., Gendrin, M., Wyer, C.A.S., and Christophides, G.K. (2017). Microbiota-induced peritrophic matrix regulates midgut homeostasis and prevents systemic infection of malaria vector mosquitoes. PLoS Pathog. *13*, e1006391.

Ruohola, H., Bremer, K.A., Baker, D., Swedlow, J.R., Jan, L.Y., and Jan, Y.N. (1991). Role of neurogenic genes in establishment of follicle cell fate and oocyte polarity during oogenesis in Drosophila. Cell *66*, 433–449.

Salazar, M.I., Richardson, J.H., Sanchez-Vargas, I., Olson, K.E., Beaty, B.J., et al. (2007). Dengue virus type 2: replication and tropisms in orally infected Aedes aegypti mosquitoes. BMC Microbiol *7*, 9.

Sanchez-Vargas, I., Harrington, L.C., Doty, J.B., Black, W.C.t., Olson, K.E., et al. (2018). Demonstration of efficient vertical and venereal transmission of dengue virus type-2 in a genetically diverse laboratory strain of *Aedes aegypti*. PLoS Negl Trop Dis *12*, e0006754.

Schwenke, R.A., Lazzaro, B.P., and Wolfner, M.F. (2016). Reproduction-immunity trade-offs in insects. Annu. Rev. Entomol. *61*, 239–256.

Shin, S.W., Zou, Z., and Raikhel, A.S. (2011). A new factor in the Aedes aegypti immune response: CLSP2 modulates melanization. EMBO Rep. *12*, 938–943.

Simmons, L.W. (2011). Resource allocation trade-off between sperm quality and immunity in the field cricket, Teleogryllus oceanicus. Behav. Ecol. *23*, 168–173.

Sirohi, D., and Kuhn, R.J. (2017). Zika virus structure, maturation, and receptors. J. Infect. Dis. *216*, S935–S944.

Souza-Neto, J.A., Powell, J.R., and Bonizzoni, M. (2019). Aedes aegypti vector competence studies: a review. Infect. Genet. Evol. *67*, 191–209.

Spradling, A.C. (1993). Germline cysts: communes that work. Cell *72*, 649–651.

Sri-In, C., Weng, S.C., Chen, W.Y., Wu-Hsieh, B.A., Tu, W.C., Shiao, S.H., et al. (2019). A salivary protein of *Aedes aegypti* promotes dengue-2 virus replication and transmission. Insect Biochem Mol. Biol. *111*, 103181.

Thornberry, N.A., and Lazebnik, Y. (1998). Caspases: enemies within. Science *281*, 1312–1316.

Wang, H., and Clem, R.J. (2011). The role of IAP antagonist proteins in the core apoptosis pathway of the mosquito disease vector Aedes aegypti. Apoptosis *16*, 235–248.

Tree, M.O., Londono-Renteria, B., Troupin, A., Clark, K.M., Colpitts, T.M., and Conway, M.J. (2019). Dengue virus reduces expression of low-density lipoprotein receptor-related protein 1 to facilitate replication in *Aedes aegypti*. Sci. Rep. *9*, 6352.

Wang, S.F., Chang, K., Loh, E.W., Wang, W.H., Tseng, S.P., Lu, P.L., Chen, Y.H., and Chen, Y.A. (2016). Consecutive large dengue outbreaks in Taiwan in 2014-2015. Emerg. Microbes Infect. *5*, e123.

Wang, S., Dos-Santos, A.L.A., Huang, W., Liu, K.C., Oshaghi, M.A., Wei, G., Agre, P., and Jacobs-Lorena, M. (2017). Driving mosquito refractoriness to Plasmodium falciparum with engineered symbiotic bacteria. Science *357*, 1399–1402.

Wasilauskas, B.L., Floyd, J., and Roberts, T.R. (1974). Use of sodium polyanethol sulfonate in the preparation of 5 per cent sheep blood agar plates. Appl. Microbiol. *28*, 91–94.

Watanabe, A., Miyazawa, S., Kitami, M., Tabunoki, H., Ueda, K., and Sato, R. (2006). Characterization of a novel C-type lectin, Bombyx mori multibinding protein, from the B. mori hemolymph: mechanism of wide-range microorganism recognition and role in immunity. J. Immunol. *177*, 4594–4604.

Wicker, C., Reichhart, J.M., Hoffmann, D., Hultmark, D., Samakovlis, C., and Hoffmann, J.A. (1990). Insect immunity. Characterization of a Drosophila cDNA encoding a novel member of the diptericin family of immune peptides. J. Biol. Chem. *265*, 22493–22498.

Williams, M., Mayer, S.V., Johnson, W.L., Chen, R., Volkova, E., Vilcarromero, S., Widen, S.G., Wood, T.G., Suarez-Ognio, L., Long, K.C., et al. (2014). Lineage II of Southeast Asian/American DENV-2 is associated with a severe dengue outbreak in the Peruvian Amazon. Am. J. Trop. Med. Hyg. *91*, 611–620.

Wu, P., Sun, P., Nie, K., Zhu, Y., Shi, M., Xiao, C., Liu, H., Liu, Q., Zhao, T., Chen, X., et al. (2019). A gut commensal bacterium promotes mosquito permissiveness to arboviruses. Cell Host Microbe *25*, 101–112 e5.

Wurzer, W.J., Planz, O., Ehrhardt, C., Giner, M., Silberzahn, T., Pleschka, S., and Ludwig, S. (2003). Caspase 3 activation is essential for efficient influenza virus propagation. EMBO J. *22*, 2717–2728.

Xi, Z., Ramirez, J.L., and Dimopoulos, G. (2008). The Aedes aegypti toll pathway controls dengue virus infection. PLoS Pathog. *4*, e1000098.

Xiao, X., Liu, Y., Zhang, X., Wang, J., Li, Z., Pang, X., Wang, P., and Cheng, G. (2014). Complement-related proteins control the flavivirus infection of Aedes aegypti by inducing antimicrobial peptides. PLoS Pathog. *10*, e1004027.

Xu, T., Caron, L.A., Fehon, R.G., and Artavanis-Tsakonas, S. (1992). The involvement of the Notch locus in Drosophila oogenesis. Development *115*, 913–922.

Yang, J., Schleicher, T.R., Dong, Y., Park, H.B., Lan, J., Cresswell, P., Crawford, J., Dimopoulos, G., and Fikrig, E. (2019). Disruption of mosGILT in Anopheles gambiae impairs ovarian development and Plasmodium infection. J. Exp. Med. *217*, e20190682.

Yen, P.S., James, A., Li, J.C., Chen, C.H., and Failloux, A.B. (2018). Synthetic miRNAs induce dual arboviral-resistance phenotypes in the vector mosquito Aedes aegypti. Commun. Biol. *1*, 11.

Yung, C.F., Lee, K.S., Thein, T.L., Tan, L.K., Gan, V.C., Wong, J.G.X., Lye, D.C., Ng, L.C., and Leo, Y.S. (2015). Dengue serotype-specific differences in clinical manifestation, laboratory parameters and risk of severe disease in adults, Singapore. Am. J. Trop. Med. Hyg. *92*, 999–1005.

Yunger, E., Safra, M., Levi-Ferber, M., Haviv-Chesner, A., and Henis-Korenblit, S. (2017). Innate immunity mediated longevity and longevity induced by germ cell removal converge on the C-type lectin domain protein IRG-7. PLoS Genet. *13*, e1006577.

Zhang, R., Zhu, Y., Pang, X., Xiao, X., Zhang, R., and Cheng, G. (2017). Regulation of antimicrobial peptides in Aedes aegypti Aag2 cells. Front. Cell. Infect. Microbiol. *7*, 22.

Zou, Z., Shin, S.W., Alvarez, K.S., Kokoza, V., and Raikhel, A.S. (2010). Distinct melanization pathways in the mosquito Aedes aegypti. Immunity *32*, 41–53.

iScience, Volume *23*

Supplemental Information

C-Type Lectins Link Immunological and Reproductive Processes in *Aedes aegypti*

Hsing-Han Li, Yu Cai, Jian-Chiuan Li, Matthew P. Su, Wei-Liang Liu, Lie Cheng, Shu-Jen Chou, Guann-Yi Yu, Horng-Dar Wang, and Chun-Hong Chen

Supplemental Data

Table S1. Primer designs for plasmid assembly, related to Figure 1

pBFv-*Aae*U6_*GCTL-3*-sgRNA vector

No	Name	Sequence
1	sgRNA of *GCTL-3*	**5'-**GCCCAGTTGGTGTAGTTGACGGG**-3'**
2	*Ae*U6-gRNA-F1	**5'-**GCTTGATATCGAATTCCTATATAATTTAATTCCACTAGAGT**-3'**
3	*Ae*U6-gRNA-R1	**5'-**TAGCTCTAAAACGGAGACGAACTCCGTCTCCATTTCACTAC TCTTGCCTCTGCTCTTATA**-3'**
4	*Ae*U6-gRNA-R2	**5'-**TTTCAAGTTGATAACGGACTAGCCTTATTTTAACTTGCTATTT CTAGCTCTAAAACGGAG**-3'**
5	*GCTL-3*-sgRNA-F	**5'-**AAATGCCCAGTTGGTGTAGTTGAC**-3'**
6	*GCTL-3*-sgRNA-R	**5'-**AAACGTCAACTACACCAACTGGGC**-3'**

pCR2-TOPO-*GCTL-3*-attp-loxp-Pub-eGFP HR donor vector

No	Name	Sequence
7	*Ae*Pub-pr-F	**5'-**GCTAGCTCTACCTAGGTATCTTTACATGTAGCTTGTGCATTG AATCC**-3'**
8	*Ae*Pub-pr-R	**5'-**AGACCTCATGCGGCCGCGTTGAAATCTCTGTTGAGCAGAA AAA GAAACGAG**-3'**
9	*GCTL-3*-up-F	**5'-**ATCCACTAGTGCTAGCTCAGTTTGCAATAAGCATTCAGCTT GTCTG**-3'**
10	*GCTL-3*-up-R	**5'-**CTGACCTGGGCCCGGGGACGTGCTGTCCCGTTGCGTGCC ATATGAA**-3'**
11	*GCTL-3*-down-F	**5'-**TCTGACCTGGGCATATGAACTACACCAACTGGGCGTTGAAT ATGCCG**-3'**
12	*GCTL-3*-down-R	**5'-**TAGATGCATGCTCGAGACAATGGACGTCTTGTGTCCTACTT ATCTC**-3'**

Table S2. Efficiency of microinjection for generation of germline mutants, related to Figure 1 and Figure S2

G0*				G1† adult		
Embryos	Larvae	Survival	Fluorescent	adult	Visible eGFP	Germline mutant
795	**210**	**26%**	**168 (80%)**	**176**	**8 (4.5%)**	**2 (1.1%)**

*G0: G0 generation., †G1: G1 generation

Table S3. Primer designs for digital droplet PCR, related to Figure 1

No	Name	Sequence
1	**Rf-nk_ddPCR-F**	**5'-**CGTGGTGCAGATAGTGAACG**-3'**
2	**Rf-nk_ddPCR-R**	**5'-**CATGTTAAGTTTGCCATAAAATTCG**-3'**
3	**Rf-nk_ddPCR-probe**	**5'-**/Hex/TGGTGACTT/ZEN/GGGAAGGATGAAGTA/3IABkFQ/**-3'**
4	**eGFP_ddPCR-F**	**5'-**CAACGAGAAGCGCGATCA**-3'**
5	**eGFP_ddPCR-R**	**5'-**CGCGATATTACTTGTACAGCTC**-3'**
6	**eGFP_ddPCR-probe**	**5'-**/56-FAM/CCTGCTGGA/ZEN/GTTCGTGACCGCC/3IABkFQ/**-3'**
7	***GCTL-3*_ddPCR-F**	**5'-**CATGGAAGGGAAATTCATATGG**-3'**
8	***GCTL-3*_ddPCR-R**	**5'-**GGGTGTATTCTTGGTAGGC**-3'**
9	***GCTL-3*_ddPCR-probe**	**5'-**/56FAM/CCGTCAACT/ZEN/ACACCAACTGGGCGT/3IABkFQ/**-3'**

Table S4. Primer designs for PCR and sequencing, related to Figure 1 and Figure S1

No	Name	Sequence	region
1	mt*GCTL-3*_F1	**5'**-CGACCATCTTCGATTTGCAGTG-**3'**	**L arm forward**
2	mt*GCTL-3*_R1	**5'**-GTGCAGTCAGCAAAGTGACG-**3'**	**L arm reverse**
3	wt*GCTL-3*_F2	**5'**-ATCGGCGCGGTAGAATACTG-**3'**	**L arm to Pub promoter**
4	wt*GCTL-3*_R2	**5'**-TTAGTCAAAAGCGCAATCGGC-**3'**	**L arm to genome**
5	mt*GCTL-3*_F3	**5'**-CCGACAACCACTACCTGAGC-**3'**	**R arm forward**
6	wt*GCTL-3*_R3	**5'**-CCAATATGCAGGGAAAAAGCAGG-**3'**	**R arm reverse**
7	wt*GCTL-3*_F4	**5'**-ATTCGGGAGAACCGAAAGGA-**3'**	**R arm to genome**
8	wt*GCT-L3*_R4	**5'**-TCTTTATCTGGTGCAAAGTGCT-**3'**	**R arm to eGFP**

Table S5. Survival data: Survival probabilities at 12 days after experiment start, related to Figure 3

	Median	SE	Lower bound	Upper bound
Control untreated	0.979	0.0147	0.951	1
Control treated	0.853	0.0364	0.784	0.927
Mutant untreated	0.937	0.0250	0.889	0.987
Mutant treated	0.905	0.0300	0.848	0.966

Table S6. Primer designs for C-type lectin real-time PCR analysis, related to Figure 1 and Figure S1

Gene	Name	sense primer sequence	antisense primer sequence
AAEL029058	***GCTL3***	ACAGCCCGTCAACTACACCAAC	CCACAACGACTCAGAAAATCAG
AAEL018265	***CTL9***	GGCGGGGAACAATCAAAAGC	CGATTTCCAGTTCAAGCCTCG
AAEL009338	***CTL10***	ATGGAGCTTACGTGGGATTG	GCCGAGTTTTACTGGGATTG
AAEL008299	***CTL11***	AATCTGGTCATGGTGGGTTC	CAGTGGAAGTTTCCCAGCTC
AAEL008681	***CTL12***	TTCGCTGGCATAAACTGTTG	ACTGCATTCTGCGAGATGTG
AAEL012353	***CTL15***	GCACTCATGCTCAATCCAAG	CCTTTACTACGGCGTTGTGC
AAEL005482	***CTL18***	GTACCCCATTCGGACACTTG	TTTCGGGCTGTAAACTGAGG
AAEL011404	***CTL19***	TGGATATTTCGGTGTTTGGCTTGG	AGTTCTCGCCGTATTCGCTAGG
AAEL013853	***CTLGA2***	GCCAACAGAATTATCCACGAGC	CGTCTAGCCAGTCCTTTTCGG
AAEL011070	***CTLGA3***	TCTGCCTAGCCGAACCAAAG	AATAATTGTGTCCACGGTACTGG
AAEL005641	***CTLGA5***	AACATTTTTCCATTGGCACTCA	ACATTCCCTATCGTTCCACTTC
AAEL014382	***CTLMA14***	TCCCCTAAGAAATCAGACGGTG	GTCATTCCCATTCCATTGCAGT
AAEL009496	***RPS7***	CAACAGCAAGAAGGCTATCG	TTGCCGGAGAACTTCTTTTC

Table S7. Primer designs for reverse transcription PCR in JAK/STAT, Toll, IMD, autophagy, RNAi, and apoptosis pathways, related to Figure 4.

Gene	Name	sense primer sequence	antisense primer sequence
AAEL012471	***Dome***	AAACGGTGGCAAAATGAACT	CTCCAGACCGGTGAGATTGT
AAEL012553	***Hop***	CCGGACTTTATCGAGCTGTC	ATCTGGTTCACTCCGTCGTC
AAEL007768	***MyD88***	GGCGAGGGTTGTTTCAAGTA	TCCCATCTGTCGATTAAGCC
AAEL010083	***IMD***	TCATTCCGCGAAGGGCTGGC	AGCGCAGAAACATCGTTCGCA
AAEL004522	***GAM***	CGGACCATCAAGCATTTCTCAA	CCAGACGGTGGGTAGAACA
AAEL007696	***REL 1***	GACTCGTCGGAGCTGAAATC	CGGTTTGTTCAGGTTGTTGA
AAEL000709	***Cactus***	TCTTGCGTTGAAGTGAGTGG	GACCCTCTGAAAGGGAAAGG
AAEL006794	***Dcr 2***	CGGGCAAACCCTGTTACATC	TGTTGGATCCTGCGCAAAC
AAEL000200	***Vago 1***	GCATTTGCCGGTCAGAGC	CTCTTCATCGGGATCGAG
AAEL003849	***DEFE***	CCCGAAAGGACCAACCATGA	TTTGCAAAAGGGCGAGCTTC
AAEL003389	***Attacin***	GGACTCCGGCGATTAAGGAG	TCTTCTTGGACCCGAAACGG
AAEL004833	***Diptericin A***	CCAATTCAGGAAGTGGAACC	TGTTGATGGGTAGCTCCAAA
AAEL013441	***Toll9A***	TCAGTCGATGGTGCCAGTTC	CGTGGCCACTTGATGTAGGT
AAEL015099	***PIAS***	GCTGCAACGCATGAAAACTA	CAGACGGGACAGTTCCAAGT
AAEL017251	***argonaute-2***	ACAACAGCAACAATCCCAGA	GTGGACGTTGATCTTGTTGG
AAEL002286	***APG 5***	CCAGGACTTGTTGGAGGACT	GTCCGGATAGCTGAGGTGTT
AAEL014148	***dredd***	GTGGCTGTTATGCGAGAAGA	AGCGTAGTTCTGCCTGAGGT
AAEL001932	***FADD***	GGGACCGTCGAACACTTCTT	CACTCAGCTGCATTAACCGC
AAEL000718	***vir-1***	GCCAAAGTCCGGTATTCTTC	TTCACGAGATCGTCAAGGTAA
AAEL027860	***Caspar***	GAATCCGAGCGAGCCGATGC	CGTAGTCCAGCGTTGTGAGGTC
AAEL005963	***Casp-3***	CGACCCAAAGCAAGGACTCA	CAGCTGCAATCGTCAAACCC
AAEL020559	***STAT***	CACACAAAAAGGACGAAGCA	TCCAGTTCCCCTAAAGCTCA
AAEL019728	***SOCS36E***	CCACTGTTTGGTGCCGGATTTGC	GCGTGCAGCGACCGGTTGTA
AAEL007624	***REL 2***	TACGAGCTCCTTCAACATGC	AGGTCTGCAGTTGACCCTCT
AAEL004223	***Cec B***	GCTGAAGAAGCTGGGAAAAAAG	CTTCCCAGTCCCTTGATGCC
AAEL000611	***Cec E***	CGAAGCCGGTGGTCTGAAG	ACTACGGGAAGTGCTTTCTCA
AAEL015515	***Cec G***	GTTATTTCTCCTGATCGCCG	CTCGTTTTCCTGCACCTCCC
AAEL000621	***Cec N***	CGGCAAGAAATTGGAAAAAGTC	GAATCGATCATCCTAGGGCC
AAEL003841	***Def A***	AACTGCCGGAGGAAACCTAT	AATGCAATGAGCAGCACAAG
AAEL003832	***Def C***	CTTTGTTTGATGAACTTCCGGAG	GAACCCACTCAGCAGATCGC
AAEL003857	***Def D***	GGCGTTGGTGATAGTGCTTG	CACACCTTCTTGGAGTTGCAG
AAEL009496	***RPs7***	GCAGACCACCATTGAACACA	CACGTCCGGTCAGCTTCTTG

Table S9. Summary of germline phenotypes. Descriptions of follicles identified in both control and mutant mosquitoes, including phenotype and % of follicles for each type identified in the two genotypes, related to Figure 7

Contents of follicle	Phenotype	Interpretation	% identified in Control (n=393)	% identified in *GCTL-3*$^{-/-}$ (n=411)
7NC*+1oc†	Follicle contains 8 cells	Normal	93.35	50.61
3NC+1oc	Follicle contains 4 cells	Follicle with clear 4 or 3+1 cells	3.33	3.41
15NC+1oc	Follicle contains 16 cells	Includes 15+1 follicle	0.95	17.27
Defect in encapsulation	Including fused follicle	Includes all abnormal nurse cells (not 3+1, 4, 7+1, 8, 15+1 and 16 follicles)	0.95	22.87
Defect in oocyte specification	Follicle contains only nurse cells	Includes 4, 8 and 16 NC (no oocyte specification)	0.24	6.57
Without germ cells	Agametic germarium	Difficult to count in mutant line	1.19	NA

*NC: nurse cells., †oc: oocyte

Table S10. Primer designs for dsRNA, related to Figure 8.

Gene	Name	primer sequence
AAEL003389	***Attacin*-F**	TAATACGACTCACTATAGGGCCGGAATTTTCGGTTCCCAC
AAEL003389	***Attacin*-R**	TAATACGACTCACTATAGGGCCGGTTGAGTTCGGCTTTTG
AAEL004522	***Gambicin*-F**	TAATACGACTCACTATAGGGTAAGAAGCTGCAGTGACTGTCAGAAGCGGT
AAEL004522	***Gambicin*-R**	TAATACGACTCACTATAGGGTTCTTCAATATCAATCAATGACACACATGCCC
pUC19 DNA	**LacZ-F**	TAATACGACTCACTATAGGGTGACCATGATTACGCCAAGC
pUC19 DNA	**LacZ-R**	TAATACGACTCACTATAGGGATGCGGCATCAGAGCAGATT

Table S11. Results of two-way ANOVA on dsRNA experiment. Significant differences between groups are bolded, related to Figure 8.

Egg laying

Group	Difference	lwr	upr	Adj P val
GCTL:ATT-Control:ATT	-12.09578544	-27.416993	3.2254225	0.2409433
Control:Cont-Control:ATT	-4.28544061	-17.066909	8.4960281	0.9708499
GCTL:Cont-Control:ATT	-62.26624738	-75.308459	-49.2240356	**0.0000000**
Control:dsLac-Control:ATT	-2.29960317	-15.180403	10.5811963	0.9993986
GCTL:dsLac-Control:ATT	-60.02842377	-73.749344	-46.3075031	**0.0000000**
Control:GAM-Control:ATT	-0.02525253	-13.666209	13.6157035	1.0000000
GCTL:GAM-Control:ATT	-14.96031746	-30.447006	0.5263709	0.0668511
Control:Cont-GCTL:ATT	7.81034483	-6.822509	22.4431986	0.7332766
GCTL:Cont-GCTL:ATT	-50.17046194	-65.031611	-35.3093127	**0.0000000**
Control:dsLac-GCTL:ATT	9.79618227	-4.923514	24.5158787	0.4634808
GCTL:dsLac-GCTL:ATT	-47.93263833	-63.392850	-32.4724271	**0.0000000**
Control:GAM-GCTL:ATT	12.07053292	-3.318754	27.4598198	0.2485990
GCTL:GAM-GCTL:ATT	-2.86453202	-19.911291	14.1822267	0.9995965
GCTL:Cont-Control:Cont	-57.98080677	-70.207020	-45.7545937	**0.0000000**
Control:dsLac-Control:Cont	1.98583744	-10.068041	14.0397161	0.9996461
GCTL:dsLac-Control:Cont	-55.74298316	-68.690750	-42.7952165	**0.0000000**
Control:GAM-Control:Cont	4.26018809	-8.602808	17.1231846	0.9727771
GCTL:GAM-Control:Cont	-10.67487685	-25.480907	4.1311528	0.3551060
Control:dsLac-GCTL:Cont	59.96664420	47.636626	72.2966620	**0.0000000**
GCTL:dsLac-GCTL:Cont	2.23782361	-10.967403	15.4430501	0.9995734
Control:GAM-GCTL:Cont	62.24099485	49.118875	75.3631146	**0.0000000**
GCTL:GAM-GCTL:Cont	47.30592992	32.274235	62.3376251	**0.0000000**
GCTL:dsLac-Control:dsLac	-57.72882060	-70.774652	-44.6829893	**0.0000000**
Control:GAM-Control:dsLac	2.27435065	-10.687352	15.2360532	0.9994632
GCTL:GAM-Control:dsLac	-12.66071429	-27.552577	2.2311481	0.1621086
Control:GAM-GCTL:dsLac	60.00317125	46.206273	73.8000695	**0.0000000**
GCTL:GAM-GCTL:dsLac	45.06810631	29.443887	60.6923258	**0.0000000**
GCTL:GAM-Control:GAM	-14.93506494	-30.489108	0.6189781	0.0701576

Larvae hatching

Group	Difference	lwr	upr	Adj P val
GCTL:ATT-Control:ATT	-20.985441	-33.948291	-8.022590	**0.0000337**
Control:Cont-Control:ATT	-2.450958	-13.265005	8.363089	0.9971965
GCTL:Cont-Control:ATT	-68.560587	-79.595242	-57.525932	**0.0000000**

Control:dsLac-Control:ATT	-1.267460	-12.165549	9.630628	0.9999661
GCTL:dsLac-Control:ATT	-65.437726	-77.046618	-53.828835	**0.0000000**
Control:GAM-Control:ATT	-5.702525	-17.243761	5.838710	0.8035555
GCTL:GAM-Control:ATT	-22.053175	-35.156033	-8.950316	**0.0000131**
Control:Cont-GCTL:ATT	18.534483	6.154030	30.914936	**0.0001855**
GCTL:Cont-GCTL:ATT	-47.575146	-60.148754	-35.001539	**0.0000000**
Control:dsLac-GCTL:ATT	19.717980	7.264052	32.171908	**0.0000561**
GCTL:dsLac-GCTL:ATT	-44.452285	-57.532743	-31.371828	**0.0000000**
Control:GAM-GCTL:ATT	15.282915	2.262465	28.303365	**0.0092846**
GCTL:GAM-GCTL:ATT	-1.067734	-15.490525	13.355057	0.9999985
GCTL:Cont-Control:Cont	-66.109629	-76.453890	-55.765368	**0.0000000**
Control:dsLac-Control:Cont	1.183498	-9.014956	11.381951	0.9999666
GCTL:dsLac-Control:Cont	-62.986768	-73.941516	-52.032021	**0.0000000**
Control:GAM-Control:Cont	-3.251567	-14.134593	7.631458	0.9848960
GCTL:GAM-Control:Cont	-19.602217	-32.129189	-7.075245	**0.0000729**
Control:dsLac-GCTL:Cont	67.293127	56.861040	77.725214	**0.0000000**
GCTL:dsLac-GCTL:Cont	3.122861	-8.049716	14.295438	0.9898116
Control:GAM-GCTL:Cont	62.858062	51.755799	73.960324	**0.0000000**
GCTL:GAM-GCTL:Cont	46.507412	33.789511	59.225314	**0.0000000**
GCTL:dsLac-Control:dsLac	-64.170266	-75.207983	-53.132549	**0.0000000**
Control:GAM-Control:dsLac	-4.435065	-15.401603	6.531473	0.9215275
GCTL:GAM-Control:dsLac	-20.785714	-33.385307	-8.186121	**0.0000215**
Control:GAM-GCTL:dsLac	59.735201	48.062027	71.408375	**0.0000000**
GCTL:GAM-GCTL:dsLac	43.384551	30.165331	56.603772	**0.0000000**
GCTL:GAM-Control:GAM	-16.350649	-29.510495	-3.190804	**0.0043802**

Fig. S1

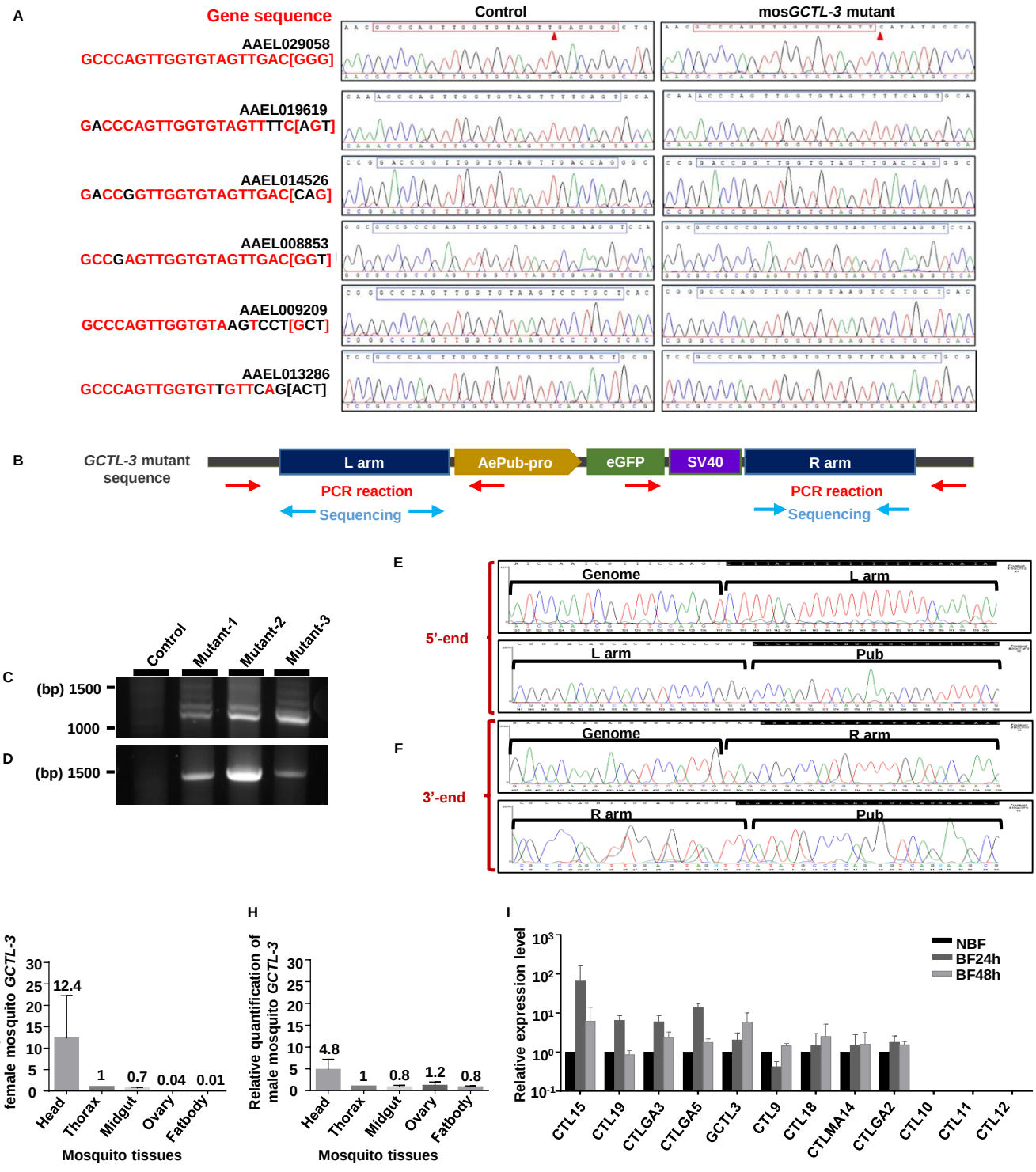
A
Gene sequence
Control
mosGCTL-3 mutant
AAEL029058
GCCCAGTTGGTGTAGTTGAC[GGG]
AAEL019619
GACCCAGTTGGTGTAGTTTTC[AGT]
AAEL014526
GACCGGTTGGTGTAGTTGAC[CAG]
AAEL008853
GCCGAGTTGGTGTAGTTGAC[GGT]
AAEL009209
GCCCAGTTGGTGTAAGTCCT[GCT]
AAEL013286
GCCCAGTTGGTGTTGTTCAG[ACT]
B
GCTL-3 mutant sequence
L arm
AePub-pro
eGFP
SV40
R arm
PCR reaction
Sequencing
PCR reaction
Sequencing
C
Control
Mutant-1
Mutant-2
Mutant-3
(bp) 1500
1000
D
(bp) 1500
E
5'-end
Genome
L arm
L arm
Pub
F
3'-end
Genome
R arm
R arm
Pub
G
Relative quantification of female mosquito GCTL-3
12.4
1
0.7
0.04
0.01
Head
Thorax
Midgut
Ovary
Fatbody
Mosquito tissues
H
Relative quantification of male mosquito GCTL-3
4.8
1
0.8
1.2
0.8
Head
Thorax
Midgut
Ovary
Fatbody
Mosquito tissues
I
Relative expression level
NBF
BF24h
BF48h
CTL15
CTL19
CTLGA3
CTLGA5
GCTL3
CTL9
CTL18
CTLMA14
CTLGA2
CTL10
CTL11
CTL12

Fig. S1. *Aedes GCTL-3* gene locus knock-out by CRISPR/Cas9, related to Figure 1, Table S1 and Table S4. (A) sequencing analyses of the five potential target sites identified for *GCTL-3* knock-out. (B) Primer sets for PCR reaction and sequencing confirmation (red and blue arrows in respectively) of break point detection. (C to D) Gel results of (C) 5'-end and (D) 3'-end break points of genomic DNA in three different *GCTL-3*$^{-/-}$ mosquito lines and detected by PCR. (E to F) Sequencing results of (E) 5'-end and (F) 3'-end break points in *GCTL-3*$^{-/-}$ mosquitoes found three *GCTL-3* mutants having an eGFP marker inserted correctly into the target site. (G) Relative quantification of mos*GCTL-3* by real time PCR in control female (N=10) and (H) male (N=10) mosquitoes as compared to whole body expression levels. Females have higher expression levels in the thorax and midgut but lower levels in the ovary and fatbody. *GCTL-3* expression level in the head was higher in females than males. Data was collected across three biological repeats; data are represented as mean ± SD. (I) Expression levels of lectins in female *A. aegypti* midgut. Data are represented as mean ± SD.

Fig. S2

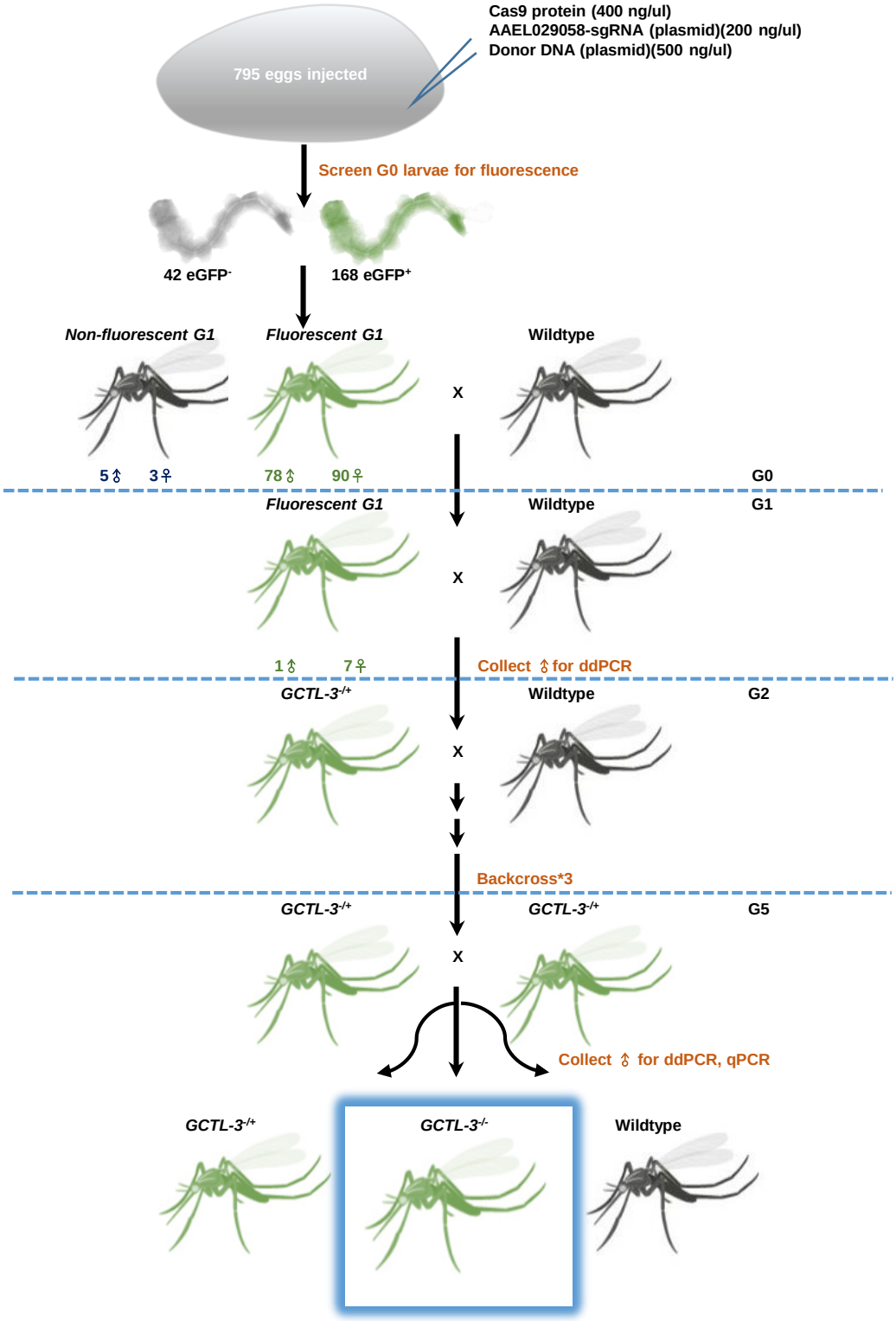

Fig. S2. Schematic of injection and screening strategies to establish an insertion of an eGFP homozygous mutant (green), related to Figure 1 and Table S2

Fig. S3

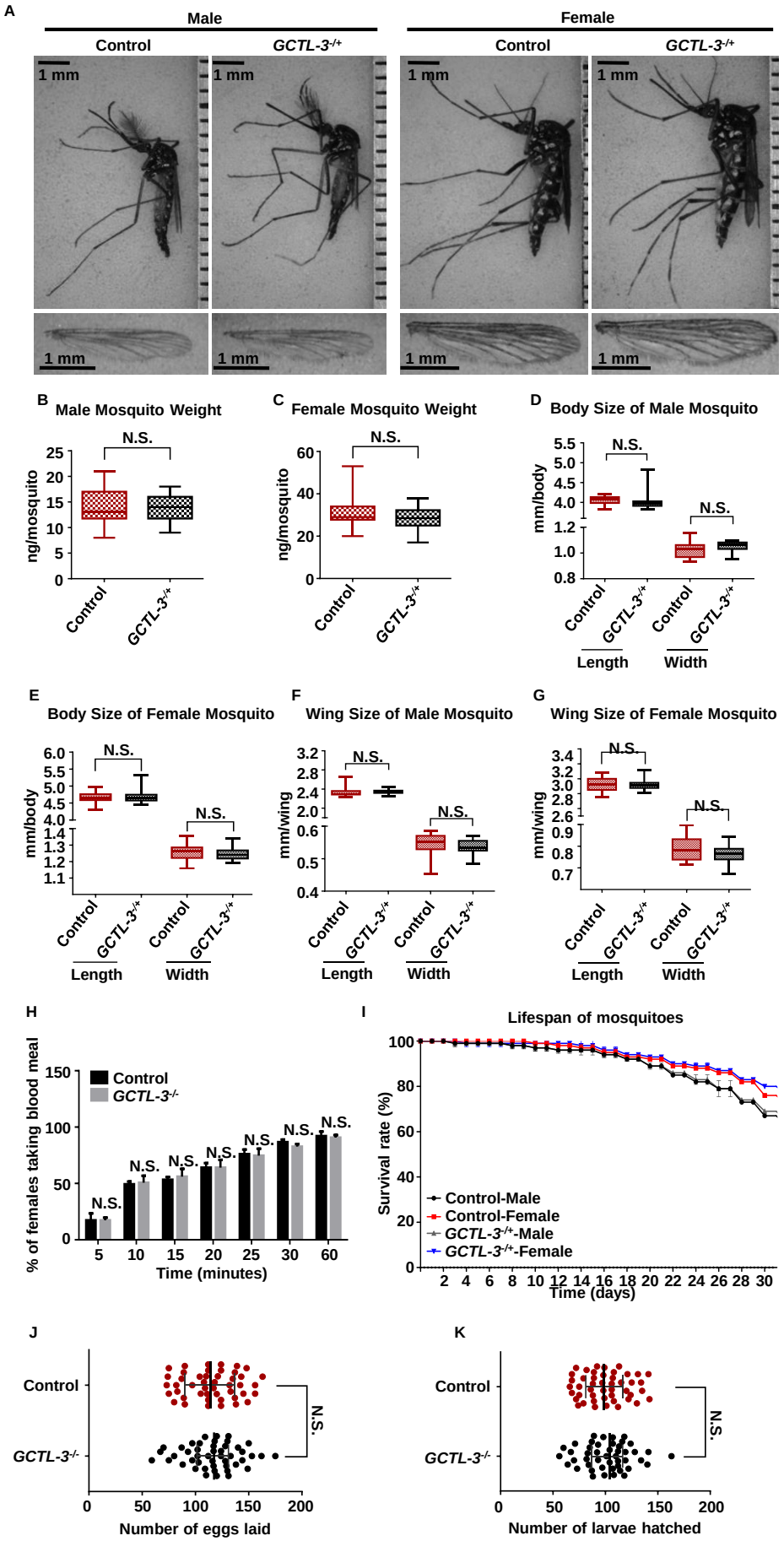
A
Male
Female
Control
GCTL-3-/+
1 mm
B
Male Mosquito Weight
ng/mosquito
N.S.
C
Female Mosquito Weight
D
Body Size of Male Mosquito
mm/body
Length
Width
E
Body Size of Female Mosquito
F
Wing Size of Male Mosquito
mm/wing
G
Wing Size of Female Mosquito
H
% of females taking blood meal
Time (minutes)
I
Lifespan of mosquitoes
Survival rate (%)
Time (days)
Control-Male
Control-Female
GCTL-3-/+-Male
GCTL-3-/+-Female
J
Number of eggs laid
K
Number of larvae hatched

Fig. S3. *GCTL-3*$^{-/+}$ mosquitoes show no change in physiology and lifespan compared to controls, related to Figure 1. (A) Phenotypes of control and *GCTL-3*$^{-/+}$ mosquitoes of both sexes. (B–G) Quantification of (B and C) mosquito weight (Sample sizes: Control/mutant females=30/30; Control/mutant males=30/30); data are represented as mean ± SD. (D and E) body size (Sample sizes: Control/mutant females=23/22; Control/mutant males=18/18) and (F and G) wing size (Sample sizes: Control/mutant females=23/23; Control/mutant males=21/21). Data are represented as mean ± SD. (H) Percentage of female control and mutant mosquitoes (N=25 for each group) identified by eye as taking a blood meal at set intervals after being provided with a blood source. All samples were taken from the same generation. Three independent experiments were conducted. Data are represented as mean ± SD. Mann-Whitney tests were used to test for potential significant differences between groups (I) Lifespans of mosGCTL-3 heterozygous mutants and control mosquitoes (N=100, two independent experiments). Data are represented as mean ± SD. (J) Number of eggs and (K) number of hatched larvae for *GCTL-3*$^{-/+}$ mutants and controls. Sample sizes: control=46; *GCTL-3*$^{-/+}$=46. Mann-Whitney tests were used to test for potential significant differences between groups. Data are represented as mean ± SD.

Fig. S4

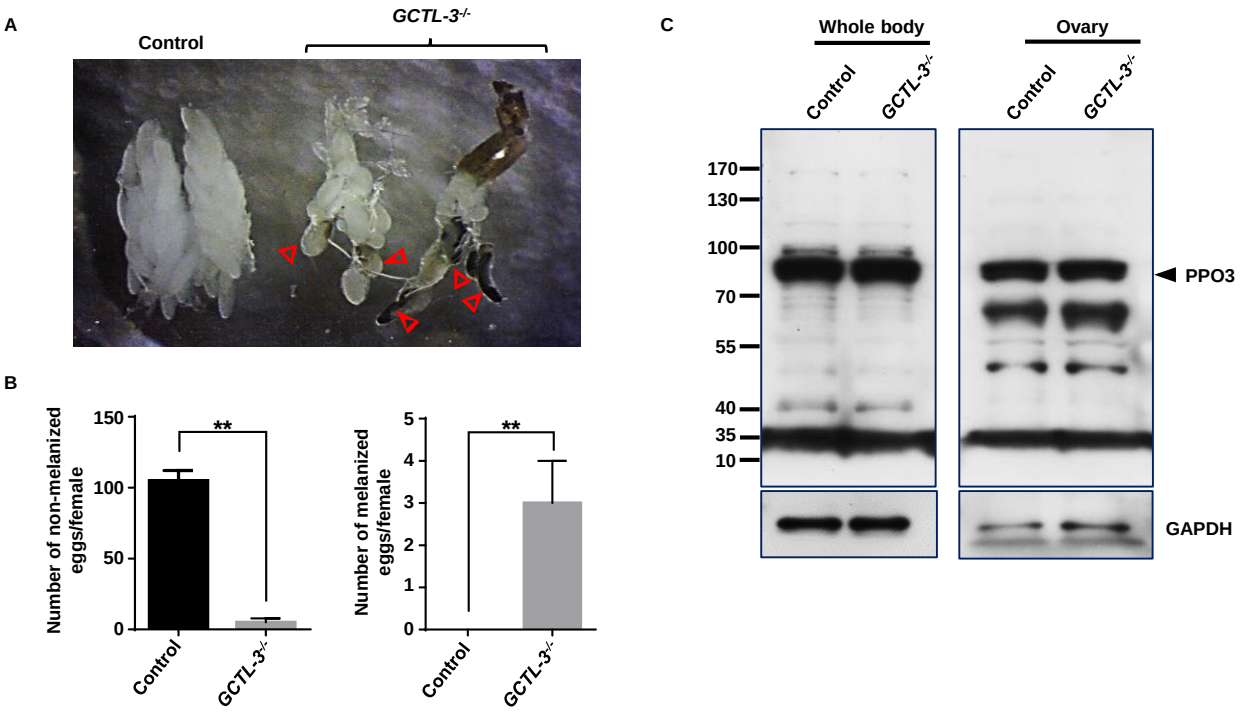

Fig. S4. Melanization in *GCTL3*$^{-/-}$ ovaries, related to Figure 5. (A) Phenotype of embryos in control (left) and *GCTL-3*$^{-/-}$ mosquitoes (middle and right). (B) Quantification of differences in egg types/counts between control and mutant mosquitoes; *GCTL-3*$^{-/-}$ mutants show significant reductions in overall egg counts (N=2) per female but have significantly greater numbers of melanized eggs (N=3) compared to controls (Student t-test; p=0.0029 and p=0.0065). Data are represented as mean ± SD. (C) PPO3 expression level in mutant and control mosquito whole bodies as well as ovaries as detected by western blotting. 40ug protein sample was used. PPO3 was the primary antibody diluted to 1:5000 in PBST containing 2% BSA; anti-rabbit was used as the secondary antibody diluted to 1:13000. GAPDH (1:10000) was used as a negative control, with anti-mouse (1:10000) the second antibody.

Fig. S5

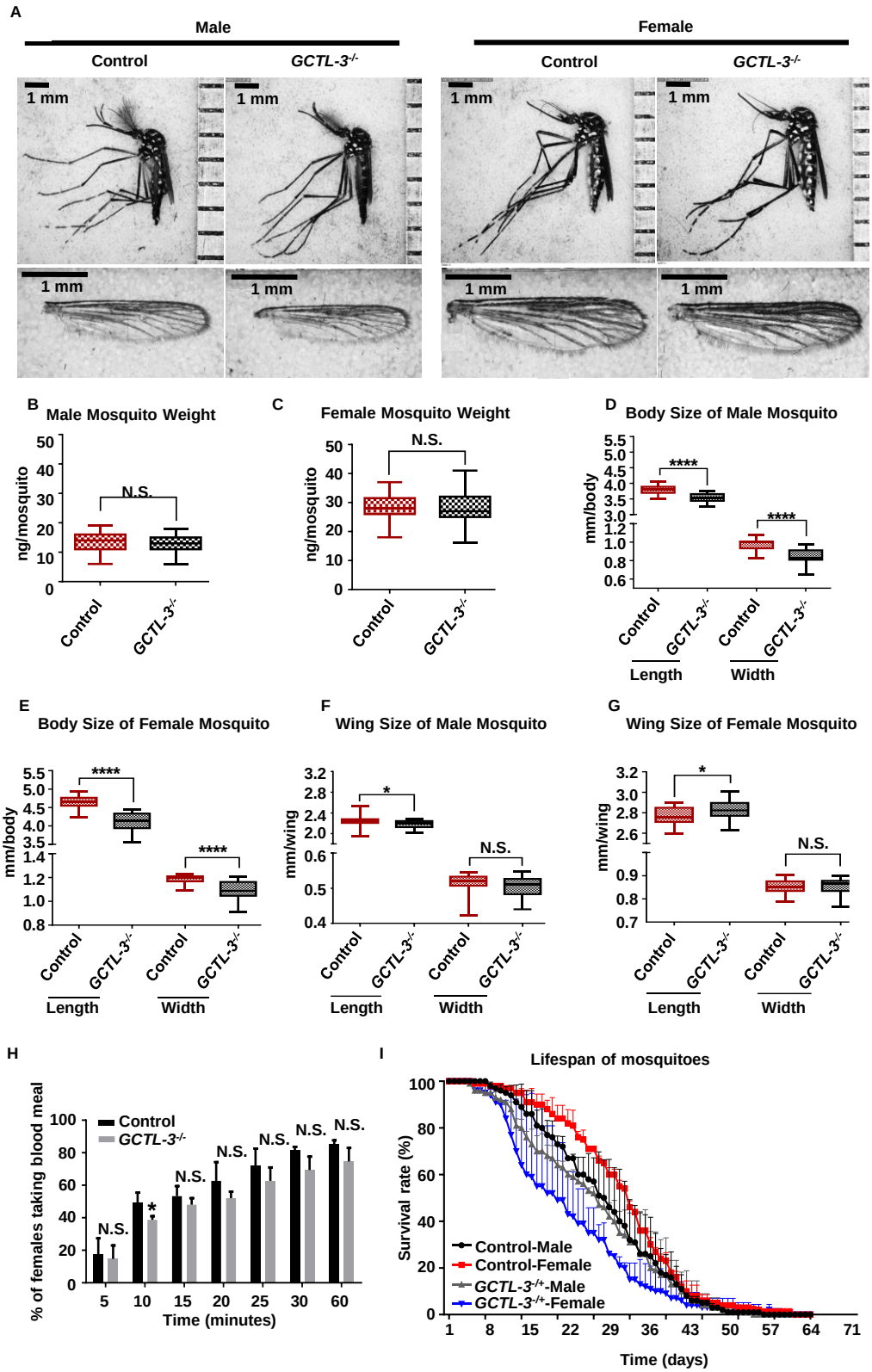
A
Male
Female
Control
GCTL-3-/-
1 mm
B
Male Mosquito Weight
ng/mosquito
N.S.
C
Female Mosquito Weight
D
Body Size of Male Mosquito
mm/body
****
Length
Width
E
Body Size of Female Mosquito
F
Wing Size of Male Mosquito
mm/wing
*
G
Wing Size of Female Mosquito
H
% of females taking blood meal
Time (minutes)
I
Lifespan of mosquitoes
Survival rate (%)
Time (days)
Control-Male
Control-Female
GCTL-3-/+-Male
GCTL-3-/+-Female

Fig. S5. *GCTL-3*$^{-/-}$ mosquitoes show change in physiology and lifespan compared to controls, related to Figure 5. (A) Phenotypes of control and *GCTL-3*$^{-/-}$ mosquitoes of both sexes. (B - G) Quantification of (B and C) mosquito weight (Sample sizes: Control/mutant females=25/25; Control/mutant males=30/30); data are represented as mean ± SD. (D and E) body size (Sample sizes: Control/mutant females=20/22; Control/mutant males=21/21) and (F and G) wing size (Sample sizes: Control/mutant females=21/23; Control/mutant males=22/21). Data are represented as mean ± SD. (H) Percentage of female control and mutant mosquitoes (total number=75 for each group) identified by eye as taking a blood meal at set intervals after being provided with a blood source. All samples taken from the same generation Three independent experiments were conducted. Data are represented as mean ± SD. Single asterisks represent a significant difference determined by the student t-test at $p<0.05$. (I) Lifespans of *mosGCTL-3* homozygous mutants and control mosquitoes (N=100, two independent experiments). Data are represented as mean ± SD.

Fig. S6

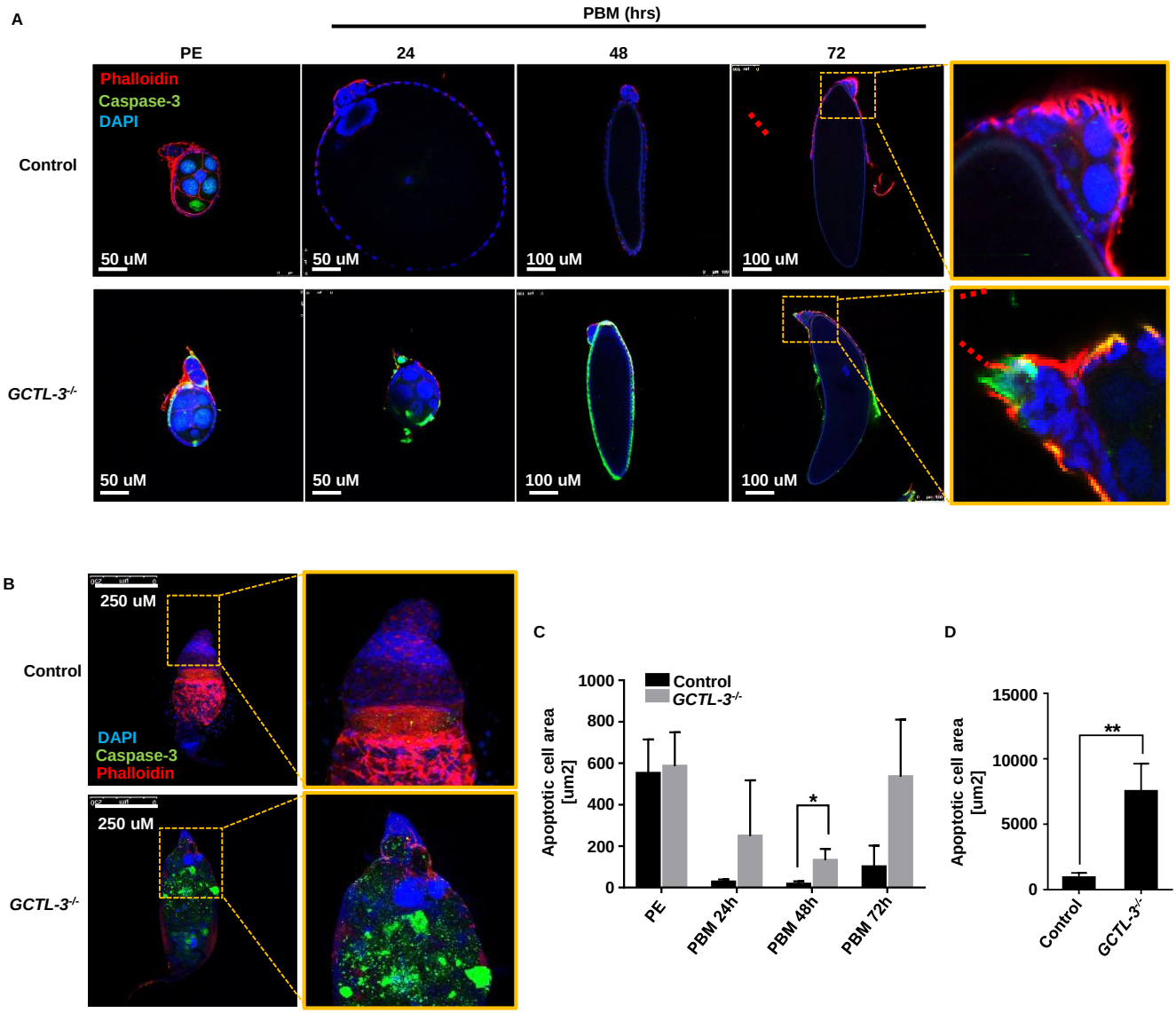

Fig. S6. Caspase-3 expression levels increased in *GCTL-3*$^{-/-}$ mutant mosquito testes and ovaries post blood meal, related to Figure 6. (A and C) 72 hours post blood meal, caspase-3 signal was increased in germ line cells of *GCTL-3* $^{-/-}$ ovaries and (B and D) testes. Data are represented as mean ± SD. Cleaved-Caspase-3 used as a primary antibody (1:500 dilution); Alexa Fluor 488 dye as a secondary antibody (1:500) as well as DAPA (1:1000) and Phalloidin (1:500) staining on the cell nucleus and cytoskeletons.

Fig. S7

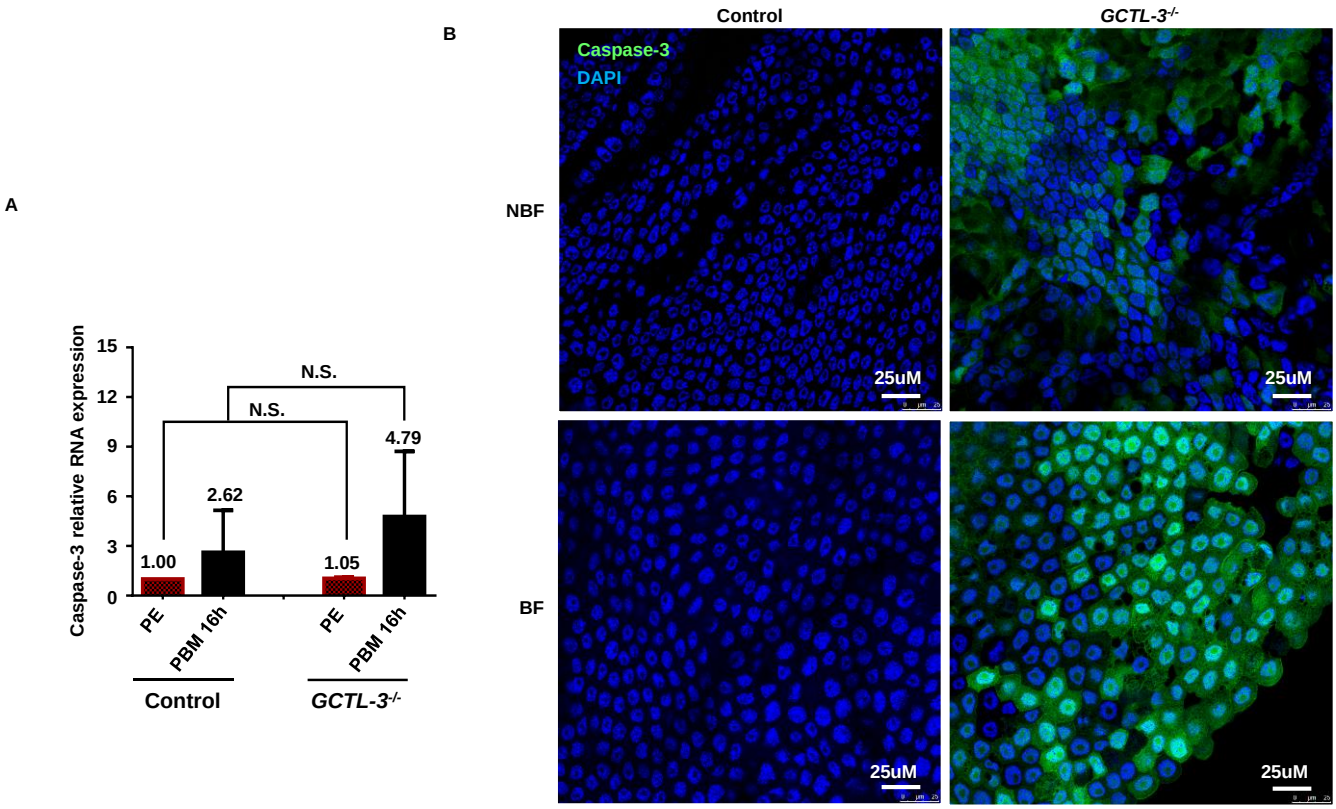

Fig. S7, see also Table S7. Cleavage Caspase-3 expression in *GCTL-3*$^{-/-}$ midguts, related to Figure 7. (A) 16 hours post blood meal, midguts of 5 day old *GCTL-3*$^{-/-}$ mosquitoes seemed to show a greater relative increase in caspase-3 RNA expression level than controls (N=10/each group), though no statistically significant difference was found (Mann-Whitney test; p=0.3333). Data are represented as mean ± SD. (B) Caspace-3 protein expression levels also appeared higher in mutant midguts than in controls, as checked via immunostaining. Primary antibody (cleave-caspase-3) was used in a 1:500 dilutions whilst second antibody (Alexa-488) was used in 1:500 dilution mixed with 1:1000 DAPI. NFB= non-blood fed; BF= blood fed.

Transparent Methods

Plasmid assembly

For the sgRNA and homologous recombination (HR) donor vector, an AaeU6 (AAEL017763) and PUb promoter were generated from *Aedes aegypti* Higgs strain genomic DNA. Detailed construction information is provided in the SI Appendix. A specific sgRNA targeting *GCTL-3* for CRISPR/Cas9 recognition was identified by copying the sequence into the flyCRISPR target finder web application (https://flycrispr.org/). An In-Fusion HD Cloning Kit (Takara Bio USA, Inc.) was used to generate the donor vector.

Mosquito rearing

All experiments used either the *Aedes aegypti* Higgs strain or mutants generated from this line. Mosquito larvae were reared at 28 °C and fed with a mixture of yeast powder (Taiwan Sugar Corporation) and goose liver powder (#7573, NTN) in a 1:1 ratio. Adults were maintained in a temperature and humidity controlled room (28 °C and ~70% RH) with a 12 hour light/dark cycle and provided with a constant 10% sucrose solution (Das et al., 2007).

Generation of mutant mosquitoes

Three days after being provided with a blood meal, female Higgs mosquitoes were allowed to lay eggs for 45 minutes. The DNA mixture used for injections was centrifuged at 13,000 rpm for 10 minutes at 4 °C. Then, 1 μL of the mixture was loaded into a glass needle (aluminosilicate tubing with filament, Sutter Instruments, AF100-64-10). The DNA mix contained 200 ng/μL sgRNA, 200 ng/μL Cas9 protein (Invitrogen, B25640), 500 ng/μL HR plasmid and 1x injection buffer (2 mM KCl, 0.1 mM sodium phosphate, pH 6.8) (Kistler et al., 2015; Kyrou et al., 2018; Nijole Jasinskiene, 2007). The tip of the glass needle was broken so that the DNA mix could be ejected. Approximately 20–60 embryos were aligned on wet filter paper and dehydrated before being transferred to a cover slide. About 200~500 μL Halocarbon oil 700 (Sigma, H8898) was used to cover all embryos. An injection needle was used to penetrate the posterior side of each embryo sequentially by moving the microscope plate laterally; care was taken that insertions did not exceed one-tenth the length of the embryonic body. Injection volume was maximally 20 pL.

Post-injection, embryos were transferred to fresh wet filter paper to remove any remaining Halocarbon oil. Injected embryos were kept on this filter paper for four days before hatching. Male and female pupae were sexed prior to adult emergence to obtain male and female virgins. Each surviving injected generation 0 (G0) male adult was outcrossed with three control females. G0 females were pooled together and crossed with control males at a male/female ratio of 1:3 (Lobo et al., 2006). Expression of *eGFP* fluorescence driven by the PUb promoter throughout the whole body of G1 *GCTL-3*$^{-/-}$ mutant mosquitoes was confirmed via use of a stereoscopic

microscope (SZX10, Olympus). Embryo survival rate following injection was 26% (N=210/795) and the success rate for generating *GCTL-3*$^{-/+}$ mutants was 1.1% (SI Appendix, Table S2).

Plasmid assembly

For the pBFv-AaeU6_*GCTL-3*-sgRNA vector, a PCR-amplified 520bp AaeU6 promoter w as generated from the AAEL017763 gene locus of *A. aegypti* genomic DNA and then f used with a sgRNA backbone sequence to obtain an AaeU6-sgRNA DNA fragment via primer extension. This AeU6-sgRNA DNA fragment was cloned into the *Eco*RI/*Not*I sites of pBFv-U6.2 plasmids to create a pBFv-AaeU6-sgRNA backbone vector for the target site single guide RNA (sgRNA) constructs for *A. aegypti* (Kondo and Ueda, 2013). A sg RNA sequence specific for *GCTL-3* for CRISPR/Cas9 recognition was identified by copy ing the sequence into a target finder web application (available at http://tools.flycrispr.mo lbio.wisc.edu/targetFinder/). 5'-GCCCAGTTGGTGTAGTTGACGGG-3' was identified as a CRISPR/Cas9 target in the *GCTL-3* coding sequence. *GCTL-3*-sgRNA fragments were g enerated by primer annealing using *GCTL-3*-sgRNA-F and *GCTL-3*-sgRNA-R. All primer s used in this study were synthesized by Integrated DNA Technologies (IDT, California, USA). The annealed *GCTL-3*-sgRNA fragments were cloned into the *Bsm*BI sites of the pBFv-AaeU6-sgRNA vector in order to generate the pBFv-AaeU6_*GCTL-3*-sgRNA plas mid. For the pCR2-TOPO-*GCTL-3*-attp-loxp-Pub-eGFP HR donor vector, a 1382bp PUb promoter was created from *Aedes aegypti* genomic DNA via PCR using AePUb-PR-F a nd AePUb-PR-Rand then cloned into the *Avr*II/*Not*I sites of a pCR2-TOPO-attp-loxp-3xp 3-eGFP HR vector to obtain the pCR2-TOPO-attp-loxp-PUb-eGFP HR vector (Anderson et al., 2010). Left and right homologous recombination flanking sequences of the *GCTL-3* gene were PCR-amplified from *A. aegypti* Higgs strain genomic DNA by using *GCTL-3*-Up-F, *GCTL-3*-Up-R, *GCTL-3*-Down-F and *GCTL-3*-Down-R (SI Appendix, Table S3).

Two PCR homology arms fragments were cloned into the *Nhe*I/*Xma*I and *Nde*I/*Xho*I sites of the pCR2-TOPO-attp-loxp-Pub-eGFP HR vector using the In-Fusion HD Cloning Kit (Takara Bio USA, Inc.) in order to generate the pCR2-TOPO-*GCTL-3*-attp-loxp-Pub-eGFP HR donor vector.

Single guide RNA design

The sgRNA targeting *GCTL-3* for CRISPR/Cas9 recognition was designed using the web tool CRISPR Optimal Target Finder on the flyCRISPR website (https://flycrispr.org/target-finder/) to identify the optimal CRISPR target sites and evaluate their specificity. A 360 bp stretch of the *GCTL-3* coding sequence was obtained from AaegL.3 *A. aegypti* genome of Vectorbase for use as the template for CRISPR target finding. The whole template sequence of *GCTL-3* was pasted into the search window. '*A. aegypti*' was selected as the reference genome for the TagScan genome searching algorithm (Iseli et al., 2007). The parameter was chosen to direct the program to identify either all CRISPR targets, CRISPR targets with 5'G for U6 promoter

driving, or CRISPR targets with 5'GG for T7 promoter driving. All sequences with similarity to CRISPR target queries on both strands of the *GCTL-3* coding sequence were identified with their specificity and location information, and a UCSC Genome Browser (http://genome.ucsc.edu/)(Kent et al., 2002) link for each potential off-target site was created. In order to generate a frameshift mutation as close as possible the ATG site, a specific CRISPR target with zero off-target effects located on the anti-sense strand of *GCTL-3*, 5'-GCCCAGTTGGTGTAGTTGACGGG-3', was selected and introduced into an AaeU6 promoter driving plasmid for sgRNA construction. The detailed user manual of CRISPR Optimal Target Finder is available at https://flycrispr.org/wp-content/uploads/2019/07/flyCRISPR-Optimal-Target-Finder-Manual-29Jul14.pdf.

PCR and sequencing

To confirm the mutant insertion site, Taq DNA polymerase (TA110150, Bernardo Scientific, Taiwan) was used to amplify the target site fragment. The PCR product was sequenced by the DNA Sequencing Core Lab at the NHRI, Taiwan by using an Applied Biosystems® 3730XL DNA Analyzer (ThermoFisher Scientific, California, USA). Construction details for all primers are included in SI Appendix, Table S4.

Characterization of insertion site by digital droplet PCR

To verify the precision of the *GCTL-3* gene knock-in and to test for potential off-target effects, a ddPCR platform was used to determine the copy number variant of *eGFP* from the *GCTL-3*-HR donor vector and *GCTL-3* alleles. Here, 20 ng of genomic DNA from a single mutant G1 or control male *Aedes aegypti* Higgs strain mosquito was used as the template for ddPCR analysis. The probe and primer sets for *eGFP* and *GCTL-3* were designed within the *eGFP* ORF and straddled the sgRNA of *GCTL-3*. AAEL006597, a known single-copy autosomal gene, was used as a reference, with the reference copy number of AAEL006597 set as two for diploid alleles (Hall et al., 2015). All of the experimental reagents and steps followed the protocol established in the ddPCR Copy Number Variation Assays Product Insert, Ver C (Bulletin #10033173) of Bio-Rad Laboratories (Mazaika and Homsy, 2014). The sequences of all primer/probe sets used in this study are included in SI Appendix, Table S5.

C-type lectin expression analysis

Adult female *A. aegypti* Higgs strain mosquitoes were fed mice blood via an artificial membrane for 30 minutes. Successfully blood fed mosquitoes were then maintained in a separate container. Midguts of these mosquitoes (N=23/group) were collected at either day one or day three post-blood meal and the total RNA was extracted using TRI reagent (Merck) following the manufacturer's protocol. cDNA was reverse transcribed from 2 μg total RNA using SuperScript III Reverse Transcriptase (ThermoFisher Scientific, California, USA) immediately after the total

RNA was extracted.

cDNA from 10 ng total RNA was used as a sample for the relative real-time PCR analysis of CTL expression. Real-time PCRs were performed using a KAPA SYBR FAST ROX Low Kit (KAPA Biosystems) on a ViiA 7 Real-Time PCR system (Thermo Fisher Scientific, California, USA). Three biological replicates were completed, and data were normalized to *A. aegypti* S7 ribosomal protein levels (RPS7; AAEL009496). Primers are listed in SI Appendix, Table S6.

DENV/ ZIKV infection of mosquitoes and virus titer determination

For oral infection, 1×10^7 PFU/mL virus stock was 1:1 mixed with mouse blood and fed to mosquitoes at 37 °C for 30 minutes via metal plate. For thoracic infection, 400 PFU virus stock was diluted with serum free medium and thoracic into adult female mosquito thorax. After seven days, a whole mosquito was collected for detecting virus titer. To determine the virus titer, 2×10^5 BHK or Vero cells were seeded into a 6-well plate and a mosquito was ground and diluted with serum-free DMEM medium. Two hours following infection, the unbound viral particles were removed and 3 mL DMEM medium containing 1% Seaplaque agarose (FMC BioProducts, Rockland, ME, US) and 2% FBS (Gibco, Paisley, UK) was added. After six days of incubation, cells were fixed and stained with 0.5 µL cell staining solution (0.5% Crystal Violet, 1.85% formaldehyde, 50% ethanol, 0.85% NaCl) and then washed with H_2O. Plaque numbers were counted and viral titer was determined as plaque forming units per mosquito.

Host seeking behavior assay

Five-to-seven day old female Higgs strain or mutant mosquitoes (N=25) were starved for 16 hours and then divided into control and experimental groups, which were kept overnight in a 15×15×15 cm cage under normal rearing conditions. A BALB/c female mouse was placed into each cage at the same time and the number of blood-fed mosquitoes (as determined by eye) was recorded every 5 minutes to 30 as well as 60 minutes. Three independent replicates were conducted.

Mosquito physiological measurements; body weight, body length, and wing length

The mosquitoes were anesthetized on ice for five minutes. Mosquitoes were transferred into 1.5 mL Eppendorf tubes after the tubes alone were weighed. A microbalance was used to weigh 25~30 mosquitoes for each group. Mosquito bodies and wings were imaged using a Dino-Lite Digital Microscope.

16S amplicon sequencing

Prior to sample collection, 5- to 7- day old female mosquitoes (N=15) were anesthetized via ice sedation for five minutes before being transferred into 1.5 mL Eppendorf tubes containing 70% ethanol for two minutes. After four washes with 1×PBS, mosquito midguts were dissected and

collected into new 1.5 mL Eppendorf tubes containing 1 mL 1×PBS within 15 minutes and stored at -20 °C. Collected samples were delivered to Tools Inc., Taiwan for DNA extraction and 16S Amplicon Sequencing.

RNA extraction and reverse transcription polymerase chain reaction (RT-PCR)

Ten non-blood fed and blood fed female Higgs strain and mutant mosquito midguts and fat-bodies were dissected in 1×PBS at room temperature. Total RNA was extracted using TRI Reagent (Sigma-Aldrich; T9424). From each sample, 1 μg total RNA was used for reverse transcription via the SuperScript™ IV Reverse Transcriptase Kit (18090010, ThermoFisher Scientific, California, USA) with random primers. RNase-free water was used to dilute cDNA 20× and 1 μL of the dilution was used for a PCR template. The design of all primers used the SYBR green system (KAPA SYBR FAST qPCR Kits, KK4600, Kapa Biosystems) and their sequences are listed in SI Appendix, Table S7.

Mosquito fertility assay

Three days after blood feeding, female mosquitoes (N=37~42) were anesthetized via ice sedation for 5 minutes before being transferred into *Drosophila* vials containing 3 mL water and 3 X 2 cm filter paper and allowed to lay eggs for 24 hours. The eggs were then counted. Eggs were subsequently hatched and larvae counted three days after egg maturation.

Mosquito survival rates following exposure to *S. marcescens*

S. marescens were cultured from the midguts of *Aedes aegypti* Higgs strain on sheep blood agar plates (BD Multipurpose Culture Medium (Sterile); Nippon Becton Dickinson Company, Ltd., Japan) and identified by VITEK 2 (bioMérieux). *S. mar* were cultured on Luria-Bertani (LB) plates and LB liquid medium was used for amplification. Mosquitoes were fed with antibiotic (10% sucrose solution including 20 units of penicillin and 20 μg of streptomycin per mL on a moistened cotton ball) for three days (Xiao et al., 2017). The mosquitoes were then starved for 16 hours before the bacterial challenge. LB or 50K/mL *S. marescens* were used to feed antibiotic-treated mosquitoes and survival rates were recorded for 12 days. To analyze survival rates we created a Cox Proportional Hazards model in which survival ~ genotype*treatment group in order to enable investigation into interactions between the variables. Survival analyses used data across two biological repeats for each group (total sample sizes=95).

Immunostaining of *A. aegypti* ovaries and midgut

The fixing and staining procedures were performed as previously described for *Drosophila* ovaries (Luo et al., 2015). In brief, 5- to 7-day-old Higgs strain or mutant mosquitoes were collected and dissected in 1×PBS to obtain ovaries or midguts. Ovaries or midguts were fixed with 4% paraformaldehyde/PBS for 20 minutes at room temperature and rinsed three times in

PBST (0.1% Triton-X in PBS). Ovaries and midguts were then blocked in 5% NGS (5% normal goat serum in PBST) for at least 30 minutes before incubation with primary antibodies (VASA, 1:500, generated in Yu Cai lab; NICD, C17.9C6, 1:50, Developmental Studies Hybridoma Bank, DSHB and Cleaved-Caspase-3 ,1:500, Cell Signaling Technology, Inc., Massachusetts, USA) diluted in 5% NGS for four hours at room temperature or overnight at 4 °C. The ovaries or midguts were then rinsed and washed with PBST for at least 30 minutes prior to incubation with secondary antibodies (Cy3-conjugated goat against mouse secondary, 1:400, Jackson Immuno Research Laboratories, Inc; Alexa Fluor 555 Phalloidin, 1:400, ThermoFisher Scientific, California, USA) diluted in PBST for 2–3 hours at room temperature.

After incubation with secondary antibodies, ovaries or midguts were rinsed and washed three times with PBST. Samples were incubated with Hoechst 33258 (Invitrogen, California, USA) for 30 minutes before being stored in Vectashield antifade mounting medium (Vector Laboratories, California, USA). Samples were mounted on slides for analysis and images were captured with a Leica SP8 upright confocal microscope. Confocal images were processed using Adobe Photoshop CS6 and Adobe Illustrator CS6 (Adobe Systems).

dsRNA synthesis and injection

dsRNA was synthesized following the MEGAscript Kit protocol. The DNA template used an T7 RNA polymerase promoter site upstream of the sequence to be transcribed (Table S8). DNA from the whole mosquito was used as a PCR template. Four reactions were utilized per gene, with each reaction having a 200 ng PCR-product template for transcription reaction assembly. dsRNA was synthesized and incubated at 37 °C for 14 hours. Phenol: chloroform extraction and isopropanol precipitation was used to purify the dsRNA, which was stored frozen at –20 °C.

Control and *GCTL-3*$^{-/-}$ female mosquitoes were exposed to the 1.5 μg dsRNA via thoracic injection (Drummond Nanoject II Auto-Nanoliter Injector) for three days. Females were allowed to lay eggs onto wet filter paper. Eggs were then counted and hatched, and the number of larvae that emerged over the next three days was also counted.

Follicle analysis

Ovaries were transferred to glass slides containing 20 μL of Vectashield antifade mounting medium. Individual ovarioles were separated using tungsten needles under a dissection microscope. A single section image or a Z-stack of images were acquired using a Leica SP8 upright confocal. A control mosquito follicle was defined as a follicle containing seven large polyploid nurse cells (NCs) and one meiotically arrested oocyte (OC), as mosquito germline stem cells/progenitors undergo three rounds of synchronized division with incomplete cytokinesis. Germ cell division will generate a follicle with 15 NCs and 1 OC, while a reduced

germ cell division will produce a follicle with 3 NCs and 1 OC. An “encapsulation defect” was defined as two consecutive follicles both containing NCs: OC ratios other than 3:1, 7:1, and 15:1. A “defect in oocyte specification” was defined as a follicle containing 4, 8, or 16 NCs without an OC, while its neighboring follicle was a control follicle. An “agametic germarium” was defined as a germarium without any VASA-positive germ cells.

Statistical analysis (Zhang et al., 2017)

Mosquitoes were randomly assigned into different groups. A significance level of $p<0.05$ was used throughout (*$p<0.05$; **$p<0.01$; ***$p<0.001$; ****$p<0.0001$). All data sets were first tested for normality using Shapiro-Wilks tests; normally distributed data sets were assessed using Two-way ANOVA whilst non-normally distributed data sets were assessed using non-parametric Mann–Whitney tests. A Cox Proportional Hazard model was used to compare the survival distributions of multiple populations. ANOVA tests were used for comparisons of egg counts and larval hatches for the *Attacin* and *Gambicin* knock-down experiments. Three biological replicates were conducted for all experiments. Statistical analysis was conducted using the GraphPad Prism 6 statistical software.

Supplemental References

Anderson, M.A., Gross, T.L., Myles, K.M., and Adelman, Z.N. (2010). Validation of novel promoter sequences derived from two endogenous ubiquitin genes in transgenic Aedes aegypti. Insect Mol Biol *19*, 441-449.

Das, S., Garver, L., and Dimopoulos, G. (2007). Protocol for mosquito rearing (A. gambiae). J Vis Exp, 221.

Hall, A.B., Basu, S., Jiang, X., Qi, Y., Timoshevskiy, V.A., Biedler, J.K., Sharakhova, M.V., Elahi, R., Anderson, M.A., Chen, X.G*., et al.* (2015). SEX DETERMINATION. A male-determining factor in the mosquito Aedes aegypti. Science *348*, 1268-1270.

Iseli, C., Ambrosini, G., Bucher, P., and Jongeneel, C.V. (2007). Indexing strategies for rapid searches of short words in genome sequences. PLoS One *2*, e579.

Kent, W.J., Sugnet, C.W., Furey, T.S., Roskin, K.M., Pringle, T.H., Zahler, A.M., and Haussler, D. (2002). The human genome browser at UCSC. Genome Res *12*, 996-1006.

Kistler, K.E., Vosshall, L.B., and Matthews, B.J. (2015). Genome engineering with CRISPR-Cas9 in the mosquito Aedes aegypti. Cell Rep *11*, 51-60.

Kondo, S., and Ueda, R. (2013). Highly improved gene targeting by germline-specific Cas9 expression in Drosophila. Genetics *195*, 715-721.

Kyrou, K., Hammond, A.M., Galizi, R., Kranjc, N., Burt, A., Beaghton, A.K., Nolan, T., and Crisanti, A. (2018). A CRISPR-Cas9 gene drive targeting doublesex causes complete population suppression in caged Anopheles gambiae mosquitoes. Nat Biotechnol *36*, 1062-1066.

Lobo, N.F., Clayton, J.R., Fraser, M.J., Kafatos, F.C., and Collins, F.H. (2006). High efficiency

germ-line transformation of mosquitoes. Nat Protoc *1*, 1312-1317.

Luo, L., Wang, H., Fan, C., Liu, S., and Cai, Y. (2015). Wnt ligands regulate Tkv expression to constrain Dpp activity in the Drosophila ovarian stem cell niche. J Cell Biol *209*, 595-608.

Mazaika, E., and Homsy, J. (2014). Digital Droplet PCR: CNV Analysis and Other Applications. Curr Protoc Hum Genet *82*, 7 24 21-13.

Nijole Jasinskiene, J.J., Anthony A. James (2007). Microinjection of A. aegypti Embryos to Obtain Transgenic Mosquitoes. In J Vis Exp.

Xiao, X., Yang, L., Pang, X., Zhang, R., Zhu, Y., Wang, P., Gao, G., and Cheng, G. (2017). A Mesh-Duox pathway regulates homeostasis in the insect gut. Nat Microbiol *2*, 17020.

Zhang, R., Zhu, Y., Pang, X., Xiao, X., Zhang, R., and Cheng, G. (2017). Regulation of Antimicrobial Peptides in Aedes aegypti Aag2 Cells. Front Cell Infect Microbiol *7*, 22.